

## Ice Nucleating Particle Measurements at 241 K during Winter Months at 3580 m MSL in the Swiss Alps

YVONNE BOOSE,\* ZAMIN A. KANJI,\* MONIKA KOHN,\* BERKO SIERAU,\* ASSAF ZIPORI,<sup>†</sup>  
 IAN CRAWFORD,<sup>#</sup> GARY LLOYD,<sup>#</sup> NICOLAS BUKOWIECKI,<sup>@</sup> ERIK HERRMANN,<sup>@</sup>  
 PIOTR KUPISZEWSKI,<sup>@</sup> MARTIN STEINBACHER,<sup>&</sup> AND ULRIKE LOHMANN\*

\* *Institute for Atmospheric and Climate Science, ETH Zürich, Zürich, Switzerland*

<sup>†</sup> *Institute of Earth Sciences, Hebrew University, Jerusalem, Israel*

<sup>#</sup> *Centre for Atmospheric Science, School of Earth, Atmospheric and Environmental Sciences, University of Manchester, Manchester, United Kingdom*

<sup>@</sup> *Laboratory of Atmospheric Chemistry, Paul Scherrer Institute, Villigen, Switzerland*

<sup>&</sup> *Empa, Swiss Federal Laboratories for Materials Science and Technology, Dübendorf, Switzerland*

(Manuscript received 12 August 2015, in final form 15 February 2016)

### ABSTRACT

Ice nucleating particle (INP) concentrations were measured at the High Altitude Research Station Jungfraujoch, Switzerland, 3580 m above mean sea level during the winter months of 2012, 2013, and 2014 with the Portable Ice Nucleation Chamber (PINC). During the measurement periods, the research station was mostly located in the free troposphere, and particle concentrations were low. At temperature  $T = 241$  K, INP concentrations in the deposition regime [relative humidity with respect to water ( $\text{RH}_w = 93\%$ )] were, on average, below 1.09 per standard liter of air ( $\text{stdL}^{-1}$ ; normalized to 1013 hPa and 273 K) and  $4.7 \pm 8.3 \text{ stdL}^{-1}$  in the condensation regime ( $\text{RH}_w = 103\%$ ) in winter 2014. The deployment of a particle concentrator upstream of PINC decreased the limit of detection (LOD) by a factor of 3 compared to earlier measurements. The authors discuss a potential bias of INP measurements toward higher concentrations if data below the LOD are disregarded and thus recommend reporting subLOD data in future publications. Saharan dust and more local, basaltic dust mixed with marine aerosol were found to constitute the dominant INP type. Bioaerosols were not observed to play a role in ice nucleation during winter because of their low concentration during this period. The INP concentrations at Jungfraujoch are low in comparison to other studies of INP at this temperature. This represents the first study addressing interannual variations of INP concentrations during winter at one location.

### 1. Introduction

The ice phase in clouds remains one of the largest challenges in predicting Earth's radiative budget accurately (Boucher et al. 2013). In the atmosphere, pure water freezes homogeneously at temperatures below 235 K (Lamb and Verlinde 2011). In mixed-phase clouds, temperatures are warmer, and supercooled water and ice coexist. Here, ice formation is initiated heterogeneously by ice nucleating particles (INPs), which represent only a small fraction of ambient aerosol particles (DeMott et al. 2003a). Conventionally, four main

pathways of heterogeneous ice nucleation are differentiated (Pruppacher and Klett 1997): First, deposition nucleation, where ice forms on an INP directly from the vapor phase. This process requires supersaturated conditions with respect to ice but can occur below water saturation. Second, condensation freezing takes place in a supersaturated environment with respect to water characterized by freezing during or after condensation of water. Third, for immersion freezing, an INP is immersed in a droplet, with the INP having potentially acted as a cloud condensation nucleus (CCN) at warmer temperatures. When the droplet is exposed to low enough temperatures it freezes. Last, contact freezing describes freezing of a supercooled droplet due to its collision with an INP. Recently, this differentiation has been questioned by some studies. Wex et al. (2014) suggest that no difference in the physical process exists between condensation and

---

Corresponding author address: Zamin A. Kanji, Institute for Atmospheric and Climate Science, ETH Zürich, Universitätsstr. 16, CH-8092 Zürich, Switzerland.  
 E-mail: zamin.kanji@env.ethz.ch; yvonne.boose@env.ethz.ch

immersion freezing. The existence of actual deposition nucleation without any intermediate water phase is questioned by Marcolli (2014).

These discussions highlight that some of the fundamental microphysical processes of ice formation mechanisms in clouds are not understood in full detail yet. However, many laboratory studies have improved our understanding of the chemical and physical nature of INPs. General requirements for INPs have been found, such as crystallinity and a size larger than approximately  $0.1\ \mu\text{m}$  in diameter (Pruppacher and Klett 1997). Certain particle types were identified to be more efficient at nucleating ice than others. Mineral dust particles have been found to be effective INPs at temperatures below about 258 K (Hoose and Möhler 2012). Recently, certain K-feldspars (i.e., endmembers of the feldspar minerals) have been discovered to be the most ice-active component of mineral dust, despite their often low abundance in these particles (Atkinson et al. 2013; Yakobi-Hancock et al. 2013). Some biological aerosols, like certain bacteria, fungal spores, and pollen, were observed to nucleate ice at temperatures above 263 K (e.g., Maki and Willoughby 1978; Levin and Yankofsky 1983; Diehl et al. 2001; Möhler et al. 2008; Attard et al. 2012). The importance of large pollen and plant debris particles for cloud processes on a global scale is debated because they require strong updrafts to reach high altitudes. However, on a more local scale during times of high biological activity, they might significantly affect cloud formation (Hoose et al. 2010). Primary biological particles associated with sea spray have gained increasing attention in recent years as field studies have suggested their ice nucleation activity plays a dominant role at remote marine locations (Bigg 1973; Wilson et al. 2015). Knopf et al. (2014) observed that the majority of INPs were associated with aged sea salt particles at a marine site close to anthropogenic and biogenic sources. Cziczo et al. (2013) found sea salt in cirrus ice crystal residuals. Particles arising from fossil fuel combustion often exhibit low to no ice nucleation activity (Phillips et al. 2013; Chou et al. 2013); however, biomass burning particles can be ice active at temperatures below 261 K (Petters et al. 2009; McCluskey et al. 2014).

In the atmosphere, microphysical and chemical processes lead to additional complexity in INP classification. Atmospheric aerosol particles are internally and externally mixed (Dall'Osto et al. 2010), and their surface can be altered by atmospheric processing (Ellison et al. 1999), by chemical reaction (Seinfeld and Pandis 2006; Pöschl et al. 2007), or by becoming coated with soluble material (Yang et al. 2011; Knopf et al. 2014). These deviations from the primary aerosol particle can significantly change its ice nucleating behavior. Sulfuric acid treatment of

mineral dust particles has been found to decrease the freezing onset temperatures (Archuleta et al. 2005; Knopf and Koop 2006; Chernoff and Bertram 2010; Sullivan et al. 2010; Yang et al. 2011; Wex et al. 2014), whereas the exposure to ammonia was found to increase the ice nucleation efficiency (Salam et al. 2007). Also, a treatment of dust particles with moderate amounts of ozone yielded higher activated fractions than those of the untreated particles (Kanji et al. 2013).

Despite these significant advancements in studying fundamental aspects of ice nucleation in the laboratory, the complexity of ice nucleation in clouds requires observational studies to quantify INP concentrations in different environments (Fan et al. 2014; Hande et al. 2015). A range of field studies exist that observed INP concentrations in ground-based studies (DeMott et al. 2003a; Klein et al. 2010; Chou et al. 2011; Ardon-Dryer and Levin 2014; Mason et al. 2016), from ship platforms (Bigg 1973), or through airborne measurements (Bigg 1967; DeMott et al. 2010; Avramov et al. 2011). Many studies have been performed by collecting aerosol particles on filters and subsequently exposing them to controlled cooling in the laboratory under sub- or supersaturated conditions with respect to water (Bigg 1967; Klein et al. 2010; Santachiara et al. 2010; Conen et al. 2012; Ardon-Dryer and Levin 2014; Knopf et al. 2014; Mason et al. 2015). Other common techniques are the use of isothermal cloud chambers or continuous flow diffusion chambers (CFDC), which allow online detection of INPs with a higher temporal resolution than the filter techniques but usually have the drawback of a higher limit of detection (LOD) (Rogers et al. 1998; Castro et al. 1998; Prenni et al. 2009; DeMott et al. 2010; Chou et al. 2011; López and Ávila 2013; McCluskey et al. 2014). Most field studies support the laboratory observations that mineral dust plays a predominant role in ice nucleation in clouds also at locations far away from potential dust emission sources (DeMott et al. 2003b; Klein et al. 2010; Cziczo and Froyd 2014). The analysis of residuals of ice crystals by means of electron-scanning microscopy and mass spectrometry has shown that there is also enrichment of mineral dust in ice residuals sampled in mixed-phase clouds in the Swiss Alps compared to the background aerosol (Kamphus et al. 2010).

The large uncertainty in representing ice clouds in global climate models (e.g., Li et al. 2012) calls for more observations of both cloud hydrometeors and INPs. So far, most existing field studies represent individual samples, restricted in space and time, while a climatology of atmospheric INPs related to dust aerosol over Europe, for example, is still missing (Hande et al. 2015). Only by understanding what controls INP concentrations at different locations as a function of temperature,

wind direction, air mass origin, and season, can we improve our knowledge of INPs. This is necessary to quantify natural variations in the present-day climate and be able to distinguish them from long-term climatic effects and feedbacks. Furthermore, to quantify the anthropogenic aerosol effect in terms of the radiative forcing of the climate system, an understanding of the potential of the natural background aerosol to form ice-containing clouds is essential (Lohmann and Kärcher 2002). This requires long-term (over periods from weeks to months) and recurrent measurements at the same locations.

To our knowledge, only two long-term studies of INP concentrations at one location exist to date. Klein et al. (2010) conducted INP concentration measurements at Mt. Kleiner Feldberg, Germany (826 m MSL). One filter was collected each day for 5 min and subsequently analyzed at temperatures between 265 and 255 K. They found similar characteristics of INPs with respect to temperature and supersaturation during a Saharan dust event compared to the rest of the year and conclude a significant role of dust in ice nucleation taking place in clouds over central Europe. Recently, Conen et al. (2015) measured INP concentrations on particulate matter with an aerodynamic diameter below 10  $\mu\text{m}$  (PM10) filters at a temperature of 265 K collected at the High Altitude Research Station Jungfraujoch in the Swiss Alps, at Mt. Chaumont, Switzerland (1171 m MSL), and at the Izaña Atmospheric Research Center on Tenerife, Canary Islands (2373 m MSL). Filters were collected over one year in 2012–13 with a temporal resolution of 24 h. They observed a strong seasonal variability of INP concentration at Jungfraujoch with values between 1 and 10  $\text{m}^{-3}$  during summer and less than 0.1  $\text{m}^{-3}$  during winter, which they attributed to enhanced scavenging processes in winter because of colder temperatures in clouds before they reach the Jungfraujoch. So far, no long-term study of INPs exists quantifying interannual variations at one location, partially because none of the sampling methods has been fully automated so far.

In this study, we present INP concentration data from winter months of three consecutive years (2012–14) with a temporal resolution of 30 min. Measurements were conducted at the Jungfraujoch in the Swiss Alps with the Portable Ice Nucleation Chamber (PINC; Chou et al. 2011). The chamber conditions were set such that deposition nucleation was studied at temperature  $T = 241$  K and a relative humidity with respect to water of  $\text{RH}_w = 93\%$  in all three years to continue the climatology of INP concentration at the Jungfraujoch started by Chou et al. (2011), who sampled in March and June 2009 at the same chamber conditions. These conditions were originally chosen to meet the onset  $T$  and  $\text{RH}$  of Saharan dust (Kanji and Abbatt 2006). At Jungfraujoch, mostly mixed-phase clouds and warmer temperatures

are observed. Therefore, condensation freezing measurements were additionally conducted in 2014 at the same temperature and  $\text{RH}_w = 103\%$ , as were deposition nucleation experiments at  $T = 247$  K.

This represents the first multiyear study addressing interannual variations in ambient INP concentrations at a location that is often in the free troposphere during winter. By utilizing an aerodynamic lens concentrator, we were able to decrease the limit of detection down to about 0.1 INP per standard liter of air ( $\text{stdL}^{-1}$ ; i.e.,  $\text{L}^{-1}$  normalized to standard temperature and pressure,  $T = 273$  K and  $p = 1013$  hPa). We examined the impact of changes in air masses, meteorological conditions, and the presence of clouds on INP concentrations. We put our findings into context with INP observations at other locations. Furthermore, we discuss the effect of excluding data below the LOD for ambient observations.

## 2. Methods

### *a. Field campaigns at the Jungfraujoch station*

INP concentrations have been measured at the High Altitude Research Station Jungfraujoch, Switzerland, (46°32'53"N, 7°59'2"E) at an altitude of 3580 m MSL. The Jungfraujoch is a Global Atmospheric Watch (GAW) station, part of the Swiss National Air Pollution Monitoring Network (NABEL), and is part of the automatic monitoring network of MeteoSwiss (SwissMetNet). A wide range of aerosol properties, trace gases, and meteorological parameters are continuously recorded by the Paul Scherrer Institute (Bukowiecki et al. 2016), Empa (Steinbacher et al. 2015), and MeteoSwiss (Appenzeller et al. 2008), respectively. The aerosol pattern at the observatory follows a yearly cycle. High particle concentrations are found in summer because of the elevation of the planetary boundary layer (PBL) and strong vertical transport processes (Baltensperger et al. 1997; Lugauer et al. 1998). In winter, particle concentrations are generally low. The observatory is considered representative for free-tropospheric conditions during 60%–68% of wintertime when thermally induced vertical transport, synoptical lifting, and foehn events are less prevalent (Zellweger et al. 2003; Herrmann et al. 2015). However, an observation deck for tourists is located two floors below the Sphinx laboratory where measurements are taken. Local emissions through tourism like cigarette smoke or helicopter flights and construction work thus may occur.

The observatory is situated in the saddle between Mt. Jungfrau to the west and Mt. Mönch to the east. The topography surrounding the Jungfraujoch is shown in Fig. 1. It favors two distinct wind directions at the site: northwest and southeast. To the north, the terrain drops



FIG. 1. Topographical map of the Jungfraujoch and the surrounding region. Mt. Jungfrau (4158 m) is located to the west and Mt. Mönch (4107 m) to the east. To the north, toward the Kleine Scheidegg pass (2061 m), the terrain falls steeply, whereas toward the south the descent over the Aletsch Glacier is far smoother. The map was modified from Google Maps ([www.google.com/maps/](http://www.google.com/maps/)).

steeply: a mostly ice-covered wall descends approximately 1500 m over a distance of 4800 m to the Lauterbrunnen valley (Ketterer et al. 2014). Toward the south, the Aletsch Glacier descends gently. During advection from the north, air from the highly populated Swiss Plateau reaches the Jungfraujoch. Air from the south is often impacted by pollution from the Po Valley but is advected over a large mountainous area before reaching the Jungfraujoch (Lugauer et al. 1998).

INP concentration measurements were taken with PINC from 12 to 27 January 2012 and within the framework of the Cloud–Aerosol Characterization Experiment (CLACE) campaigns from 21 January to 28 February 2013 (CLACE2013) and 23 January to 16 February 2014 (CLACE2014). Both CLACE campaigns aimed at observing cloud microphysical as well as aerosol properties in mixed-phase clouds and involved several international research groups. In addition to INP concentration, cloud microphysical variables were measured (Kupiszewski et al. 2015; Lloyd et al. 2015; Vochezer et al. 2016; Worrington et al. 2015). An overview of all instruments referred to in this study is given in Table 1.

### b. Ice nucleating particle concentration measurements during field campaigns

The Portable Ice Nucleation Chamber (Chou et al. 2011) is a continuous flow diffusion chamber with two parallel, vertically oriented walls. Inside the PINC chamber, a supersaturation with respect to ice is supplied by a temperature gradient between the two ice-coated walls. By changing the wall temperatures, the sample temperature and supersaturation inside the chamber are regulated. Within the aerosol layer the temperature uncertainty was

found to be 0.4 K and relative humidity uncertainty was 4% (see appendix and Kanji et al. 2013). A schematic of the PINC setup at Jungfraujoch is shown in Fig. 2. Upstream of the chamber, an impactor (orifice diameter: 0.071 cm; TSI, Shoreview, Minnesota) with a cutoff at  $D_{50} = 0.9 \mu\text{m}$  aerodynamic diameter (i.e., diameter, where 50% of the particles penetrate) is mounted to prevent larger particles from entering the chamber. This corresponds to an optical diameter of  $0.74 \mu\text{m}$  if we assume an ambient average particle density of  $1.5 \text{ g cm}^{-3}$  (Cozic et al. 2008) and that the optical diameter equals the Stokes diameter (Chou et al. 2011). As both the particle density and shape factor of the ambient aerosol are not known precisely, in the following, no conversion is applied and the respective diameters as measured by the different instruments are given.

The lower part of the PINC chamber is held at ice saturation at the temperature of the warm wall. Here, droplets evaporate, but ice crystals are preserved, allowing the differentiation by size downstream of the chamber between the larger ice crystals that grow inside the chamber and smaller interstitial aerosol particles as well as droplets. Particles and hydrometeors are counted with an optical particle counter (OPC; Lighthouse Remote 5104, Fremont, California). Particles sized above  $3 \mu\text{m}$  in diameter are classified as ice crystals. At high relative humidities, droplets grow to sizes large enough that even after the evaporation section they are larger than  $3 \mu\text{m}$  in diameter and cannot be distinguished from ice crystals. This so-called droplet breakthrough occurs at  $\text{RH}_w = 108\%$  for  $T = 241 \text{ K}$ .

The sample temperature in PINC was usually set to  $T = 241 \text{ K}$  and a relative humidity of  $\text{RH}_w = 93\%$ , which corresponds to a relative humidity with respect to ice of  $\text{RH}_i = 127\%$  ( $\text{INP}_{241\text{K},93\%}$ ). During the 2012 and 2013 measurement periods, focus was placed on one condition to be able to detect the very low INP concentrations during winter with a temporal resolution of 30 min. In January and February 2014, in addition to a continuation of the deposition mode time series at  $T = 241 \text{ K}$ , INP concentration data were frequently collected at the same temperature at  $\text{RH}_w = 103\%$ , corresponding to  $\text{RH}_i = 141\%$  ( $\text{INP}_{241\text{K},103\%}$ ). In 2013 and 2014, measurements at  $T = 248 \text{ K}$  and  $T = 247 \text{ K}$ , respectively, were conducted as well but at a lower measurement frequency. These conditions were closer to the ambient temperatures (Fig. 3d). For an overview of all measurement conditions see Table 2.

In 2013 and 2014 an aerodynamic lens concentrator (Enertech, Inc., Seattle, Washington; Novossov and Ariessohn 2014) was applied upstream of PINC to

TABLE 1. Instrumentation at Jungfraujoch.

Instrument	Model	Measured quantity
PINC	—	INP concentration, $\leq 1 \mu\text{m}$
Condensation particle counter	TSI CPC 3772	Particle concentration, $\geq 0.01 \mu\text{m}$
Condensation particle counter	TSI CPC 3010	Particle concentration, $\geq 0.01 \mu\text{m}$
Scanning mobility particle sizer	TSI DMA 3071, CPC 3775	Particle size distribution, 0.02–0.6 $\mu\text{m}$
Optical particle counter	Grimm dust monitor 1.108	Particle size distribution, 0.3–20 $\mu\text{m}$
Waveband Integrated Bioaerosol Sensor	WIBS-4	(Non)fluorescent particle size distribution, 0.8–20 $\mu\text{m}$
Betameter	Thermo ESM Andersen FH62 I-R	Mass concentration, PM10
Nephelometer	TSI 3563	Scattering coefficients
Aethalometer	Magee Scientific AE31	Absorption coefficients
Cavity ring-down spectrometer	G2401, Picarro, Inc.	CO
Chemiluminescence detector	ECO Physics CLD 89p	NO <sub>y</sub>
Particulate volume monitor	PVM-100	Liquid water content
Cloud droplet probe	CDP	Droplet size distribution
Cloud sampler	—	Cloud water

enrich the particle concentration in the sample air and thus to improve the detection of very low INP concentrations. The concentrator is based on the working principle of a virtual impactor (Kulkarni et al. 2011) with a major flow of  $10 \text{ L min}^{-1}$  and a minor (sample) flow of  $1 \text{ L min}^{-1}$ . Laboratory characterization tests using Arizona test dust particles larger than  $0.12 \mu\text{m}$  in mobility diameter did not show a clear cutoff size of the concentrator and yielded a concentration factor between 4 and 7. However, for the ambient measurements, the size and density of the INPs is not known explicitly. Hence, during the field deployment, frequent comparisons between INP concentrations during times when the concentrator was turned on (enrichment of large particles occurred) to those during an interval immediately before or after when the concentrator was turned off (enrichment not taking place) were performed. The comparisons yielded an empirical concentration factor of  $3 \pm 0.6$  for INP concentration data of the CLACE2014 campaign. During CLACE2013, the concentrator was used with the same flow setup as during CLACE2014; hence, the same concentration factor is assumed also for the CLACE2013 data. Repeated zero tests between and during the campaigns showed that the concentrator was leak-tight [condensation particle counter (CPC) showed  $< 0.05 \text{ cm}^{-3}$  over a period of several minutes when sampling filtered air].

PINC was connected to the GAW total aerosol inlet via approximately 7 m of stainless steel and conductive tubing of 6- and 8-mm inner diameter, leading to a total residence time of the aerosol particles of approximately 2 s before entering PINC. The total aerosol inlet is heated to 298 K ( $\text{RH}_w \leq 20\%$ ) to evaporate cloud droplets as well as ice crystals after being

collected (Weingartner et al. 1999). The warm temperature and low relative humidity inside the sampling tube also eliminates potential preactivation or memory effects of ice crystal residuals (Knopf and Koop 2006; Wagner et al. 2014). When mixed-phase clouds are present, the aerosol sample consists of cloud droplet residuals, ice crystal residuals as well as interstitial aerosol particles. The inlet design has an upper cutoff diameter of  $40 \mu\text{m}$ , which prevents larger hydrometeors from entering the inlet and clogging it. As a consequence, ice crystal residuals from crystals  $> 40 \mu\text{m}$  are not sampled by PINC. At an ambient temperature of 258 K and  $\text{RH}_i = 120\%$ , it takes about 3 min for an ice crystal to grow to  $40 \mu\text{m}$  in diameter, according to the equation given by Rogers and Yau (1989). Thus, the ice crystals that are small enough to enter the inlet and whose residuals are sampled are likely freshly formed. Interstitial aerosols and droplets are generally smaller and thus sampled representatively. If one assumes on average the total aerosol loading to be comparable inside and outside of clouds, a high number of ambient ice crystals larger than  $40 \mu\text{m}$  should result in significant differences between in-cloud and out-of-cloud INP concentrations.

### c. INP data analysis

The number of INPs in the atmosphere is generally low, representing only 1 in  $10^5$  atmospheric aerosol particles (Rogers et al. 1998). Hence, the detection of INPs must be approximated by Poisson statistics (Rogers et al. 2001), and the uncertainty of a measurement scales with the square root of the INP count. Each INP concentration data point presented in this study corresponds to 20 min of averaged INP counts during which the wall temperatures were kept constant

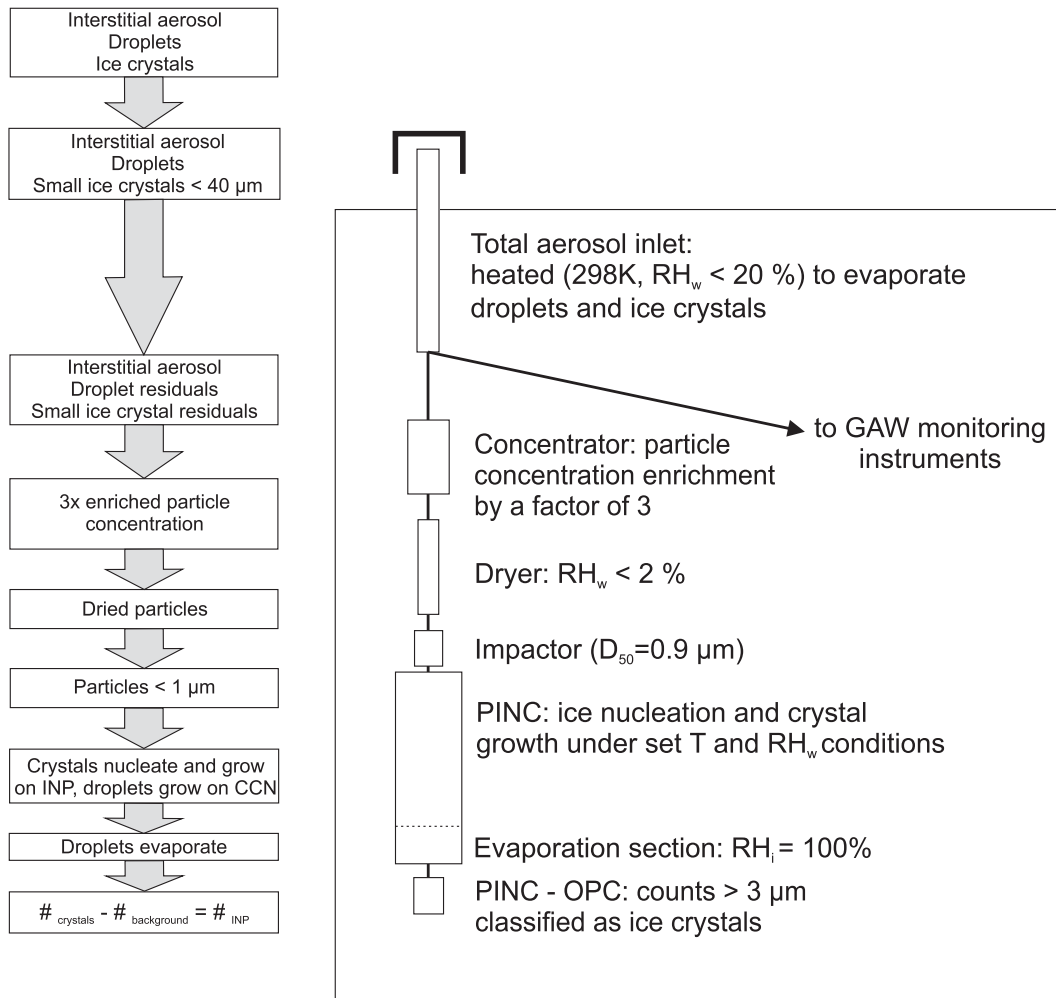


FIG. 2. Schematic of INP measurements with the PINC at the Jungfraujoch.

(for measurement conditions and total measurement times, see Table 2). Before and after each measurement, the sample air was drawn through a filter for 10 min to check the background counts of the chamber (e.g., from frost particles falling off the chamber walls). From these two filter measurement periods, the mean background was determined for the intermediary sample period. INP concentrations were calculated as the averaged counts during the sample period minus this averaged background. The background counts also follow Poisson statistics. The limit of detection is given for each measurement by the 68% confidence interval of the mean background count. The LOD depends on the temperature and humidity conditions in the chamber and changes over time after ice coating the chamber walls. As the background and thus the LOD have been observed to change only gradually and without sudden increases, a linear average between the two background periods is reasonable. The typical detection limit was

between 0.3 and 2 stdL<sup>-1</sup> in January 2012. It was lowered to 0.1–0.45 stdL<sup>-1</sup> by using the concentrator during CLACE2013 and 2014, which improved the signal to noise ratio by a factor of 3.

The ice-active surface site density is given as  $n_s$  (m<sup>-2</sup>) = INP/ $A$ , with  $A$  being the total aerosol surface area per unit volume (Connolly et al. 2009; Hoose and Möhler 2012). Losses in the tubing are expected to be minor for the size range sampled by PINC (0.1–1 μm). INPs that were too large to pass the impactor have been accounted for by  $INP_{lost} = n_s A_{lost}$ , with  $A_{lost}$  being the total surface area of particles that were omitted by the impactor derived from optical particle size distributions. In the remainder of the text, the corrected INPs concentrations (i.e., the sum of the measured INP and the calculated omitted INPs that were too large to enter PINC) are given in brackets after the measured INP concentrations. For the 2012 campaign, no size distribution measurements of particles larger than 0.6 μm were available; thus, the INPs are corrected by the

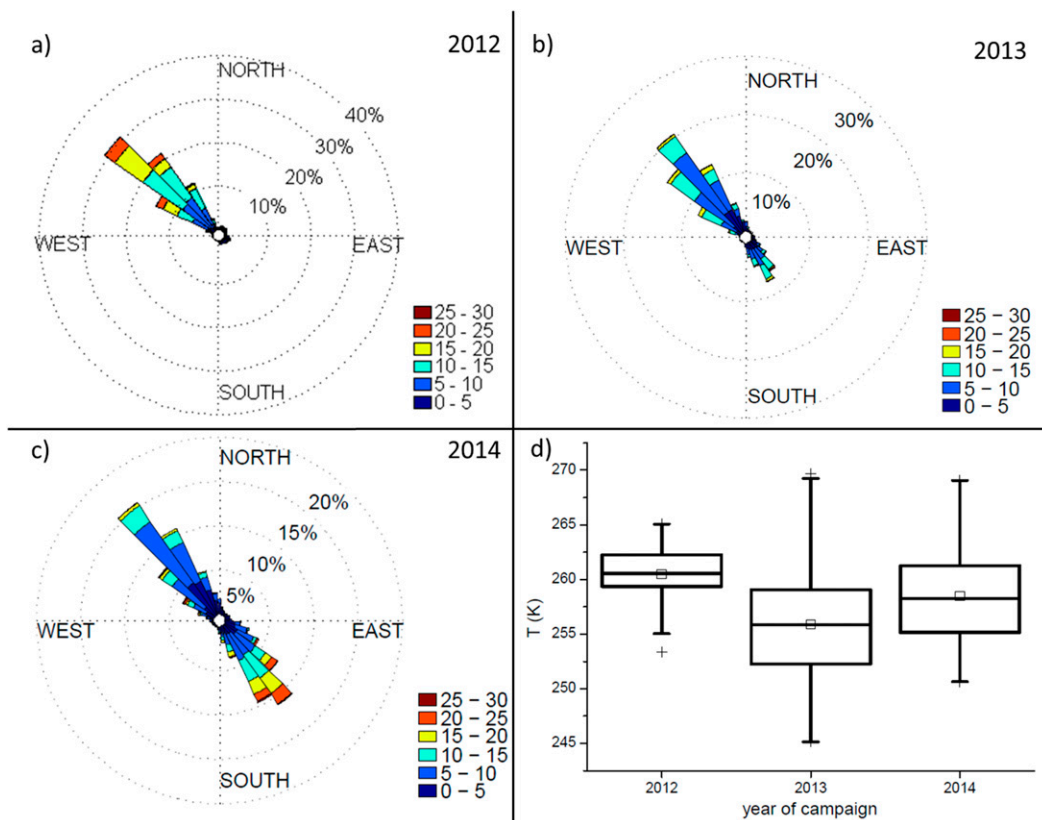


FIG. 3. (a)–(c) Wind direction distribution during the measurement periods. The color code indicates the horizontal wind velocity ( $\text{m s}^{-1}$ ). (d) Ambient temperature during the measurement periods. Median values are given as middle bars, mean values as squares. The box indicates the 25th and 75th and the whiskers the 5th and 95th percentiles. The plus signs are the minimal and maximal values.

average omitted fraction from the 2013 and 2014 measurements (10%) at the same chamber conditions. The error of the  $\text{INP}_{\text{lost}}$  is calculated based on the Poisson error of the measured INP and 40% error assumed for the aerosol particle surface measurements.

As the process when an ice crystal starts forming on an INP cannot be visually inspected in PINC, we refer to deposition nucleation when RH conditions were set to be subsaturated with respect to water where freezing processes have a low probability to occur. When

chamber conditions were above water saturation, we refer to the freezing process as condensation freezing. This may include also cases of immersion freezing. As droplet freezing processes are more efficient than deposition nucleation, the latter plays only a minor role above water saturation. More details regarding data processing and analysis as well as the characterization of the chamber are given in the [appendix](#) as well as in [Chou et al. \(2011\)](#), [Kanji et al. \(2013\)](#), and [Wex et al. \(2015\)](#).

TABLE 2. PINC measurement conditions: chamber temperature, relative humidity, and total sampling duration ( $t$ ).

	12–27 Jan 2012				21 Jan–28 Feb 2013				23 Jan–16 Feb 2014			
	$T$ (K)	$\text{RH}_i$ (%)	$\text{RH}_w$ (%)	$t$ (h)	$T$ (K)	$\text{RH}_i$ (%)	$\text{RH}_w$ (%)	$t$ (h)	$T$ (K)	$\text{RH}_i$ (%)	$\text{RH}_w$ (%)	$t$ (h)
Deposition	241	127	93	62.3	241	127	93	138.9	241	127	93	54.6
Condensation	—	—	—	—	—	—	—	—	241	141	103	28.5
Deposition	—	—	—	—	248	110	86	1	—	—	—	—
Deposition	—	—	—	—	248	123	96	0.8	247	119	93	19
Deposition	—	—	—	—	248	127	99	3.1	247	126	98	17.8

#### *d. Auxiliary instruments and data during field campaigns*

##### 1) METEOROLOGICAL DATA

Ambient temperature and relative humidity, horizontal wind direction and speed, and the occurrence of foehn situations were received for the time periods of the measurement campaigns from the Federal Office of Meteorology and Climatology (MeteoSwiss; [www.meteoswiss.admin.ch](http://www.meteoswiss.admin.ch)).

##### 2) AEROSOL NUMBER AND MASS CONCENTRATION AND SIZE DISTRIBUTION MEASUREMENTS

Total aerosol particle concentration larger than  $0.01\ \mu\text{m}$  was measured with a condensation particle counter (TSI; model CPC 3772). A scanning mobility particle sizer [SMPS; TSI; Differential Mobility Analyzer (DMA) model 3071; CPC model 3775] and an optical particle counter (Grimm dust monitor, model 1.108) measured the aerosol particle size distribution in the ranges  $0.02\text{--}0.6\text{-}\mu\text{m}$  mobility diameter and  $0.3\text{--}20\text{-}\mu\text{m}$  optical diameter, respectively. The CPC 3772, SMPS, and OPC are part of the long-term monitoring program of GAW and sampled from the GAW total aerosol inlet in parallel to PINC. All particle concentrations are given at standard conditions and were calculated by using the long-year average pressure at the Jungfraujoch Sphinx laboratory of 654 hPa and a laboratory temperature of  $T = 298\ \text{K}$ . The mass concentration of PM<sub>10</sub> is determined both in 24-h integrated high-volume samples on quartz fiber filters (sampler: DHA-80, Digitel; filters: Pallflex Tissuquartz, Pall Corporation) as well as recorded continuously. The continuous PM<sub>10</sub> observations are made with a betameter (Thermo ESM Andersen FH62 I-R), which measures the attenuation of beta radiation, emitted by a krypton-85 source, due to aerosol particles that are sampled on a filter tape.

##### 3) CLOUD PROBES: TIMES OF CLOUD PRESENCE

During CLACE2013 and CLACE2014, a particulate volume monitor (PVM-100; Gerber Scientific, Inc., United States) and a cloud droplet probe (CDP; Droplet Measurement Technologies, United States) measured cloud liquid water content (LWC). The PVM-100 measures LWC based on the scattering of light (780-nm laser) in the forward direction by an ensemble of particles passing between the transmitter and receiver arms of the instrument (Gerber 1991; Wendisch et al. 2002). The CDP is a single particle instrument that counts and sizes individual cloud droplets based on light scattering at  $4^{\circ}\text{--}12^{\circ}$  in

the forward direction by particles passing through a 658-nm laser beam (Lance et al. 2010). LWC can subsequently be calculated from the measured CDP cloud droplet size distributions. Cloud presence times during CLACE2013 and CLACE2014 were identified based on 5-min averages of LWC measured with the PVM-100 and the CDP, with the LWC threshold for classifying an in-cloud period defined as  $0.02\ \text{g m}^{-3}$ .

##### 4) WIBS-4: PARTICLE FLUORESCENCE MEASUREMENTS

From 2 to 17 February 2014, the Waveband Integrated Bioaerosol Sensor (WIBS-4; Kaye et al. 2005; Healy et al. 2012) measured single-particle fluorescence and an asymmetry factor of particles between  $0.8\text{-}$  and  $20\text{-}\mu\text{m}$  optical diameter, which can be used to infer biological aerosol concentration. This method makes use of the laser-induced fluorescence of several constituents of biological particles, such as amino acids, coenzymes, or biopolymers (Pöhlker et al. 2012). However, nonbiological aerosol particles, such as mineral dust, have also been found to fluoresce and therefore may interfere with the bioaerosol detection. The fluorescence of atmospheric mineral dust can stem from the minerals themselves or from biological material on the surface of the dust grains. For the current study, a hierarchical agglomerative cluster analysis method using the Ward linkage and  $z$ -score normalization was applied to the fluorescent population, which yielded a three-cluster solution (Crawford et al. 2016). Two of the clusters were weakly fluorescent and are consistent with mineral dust (Pöhlker et al. 2012). The third cluster was moderately fluorescent in all channels, suggesting that this was likely representative of biological material (Crawford et al. 2014). For further details of the analysis method used, see Crawford et al. (2015).

##### 5) AETHALOMETER: BLACK CARBON MEASUREMENTS

The equivalent black carbon (EBC) mass concentration was measured using an aethalometer (Magee Scientific, Berkeley, California; model AE31) via the light attenuation by aerosol particles deposited on a filter tape. The reported EBC concentrations refer to a light wavelength of 880 nm and an instrument default mass absorption cross section of  $16.6\ \text{m}^2\ \text{g}^{-1}$ .

##### 6) TRACE GAS MEASUREMENTS

From the continuous trace gas observations, measurements of total reactive nitrogen ( $\text{NO}_y$ ) and carbon monoxide (CO) were used as indicators for free-tropospheric conditions (section 3b).  $\text{NO}_y$  was measured as NO by

chemiluminescence after conversion of  $\text{NO}_y$  to NO on a heated gold catalyst (CraNOx; Ecophysics; Pandey Deolal et al. 2012). CO was measured by cavity ring-down spectroscopy (G2401; Picarro, Inc.; Zellweger et al. 2012).

#### 7) CLOUD WATER SAMPLES: STRONTIUM ISOTOPE MEASUREMENTS

Cloud water samples were taken frequently on the terrace adjoining the Sphinx laboratory during CLACE2014. Strontium (Sr) separation from the sample was done with Sr-Spec resin similar to the method described in Stein et al. (1997). The chemical analysis of the sodium, aluminum, and strontium concentrations was done with an inductively coupled plasma mass spectrometer (ICP-MS; Agilent 7500cx). The isotopic ratio of strontium ( $^{87}\text{Sr}/^{86}\text{Sr}$ )<sub>sample</sub> was measured with a multicollector inductively coupled plasma mass spectrometer (MC-ICP-MS; Neptune Plus). The marine ( $^{87}\text{Sr}/^{86}\text{Sr}$ ) ratio is known to be homogeneous in the ocean with a value of 0.709 17 (Hodell et al. 1990). Basalt and volcanic rocks have lower values, whereas granite rocks and dust from the Sahara have higher ratio values (Capo et al. 1998, and references therein). To get an indication on the geochemical origin of the aerosol sampled, we use the  $\delta 87$  parameter:

$$\delta 87 = \left[ \frac{(^{87}\text{Sr}/^{86}\text{Sr})_{\text{sample}}}{(^{87}\text{Sr}/^{86}\text{Sr})_{\text{marine}}} - 1 \right] \times 1000, \quad (1)$$

with  $(^{87}\text{Sr}/^{86}\text{Sr})_{\text{marine}} = 0.709 17$ . It describes how strongly the sample ratio differs from the marine ratio. A geographic overview of ( $^{87}\text{Sr}/^{86}\text{Sr}$ ) measurements of natural mineral waters in Europe and predicted surface geology can be found in Voerkelius et al. (2010). Comparing  $\delta 87$  to the Na/Al ratio, also commonly used as a tracer for marine aerosol, shows that a smaller Na/Al ratio corresponds to a higher absolute  $\delta 87$  [i.e., less marine air (see appendix)]. For the strontium isotope analysis, multiple cloud samples of one period had to be combined (given by the Sr sample number in Table A1). An overview of the sampling times and numbers as well as more details on the sampling and analysis of the cloud water are provided in the appendix.

#### 8) IDENTIFICATION OF SAHARAN DUST EVENTS

The presence of a Saharan dust event (SDE) at the Jungfraujoch is commonly identified by a negative single-scattering albedo exponent ( $\alpha_{\text{SSA}}$ ) during a period of at least 4 h (Collaud Coen et al. 2004). An integrating nephelometer (TSI; model 3563) measured the aerosol total scattering coefficient at three different wavelengths (450, 550, and 700 nm), while the absorption coefficients at the respective wavelengths were

retrieved from the aethalometer measurements. From these values, the single-scattering albedo (SSA) was calculated for each of the wavelengths and fitted with a power law as described by Collaud Coen et al. (2004) to obtain the single-scattering albedo exponent  $\alpha_{\text{SSA}}$ . The SSA is generally positively correlated with the wavelength for the Jungfraujoch background aerosol. However, when Saharan dust is present, it decreases with wavelength, and  $\alpha_{\text{SSA}}$  becomes negative as a result of the larger size and different composition of the Saharan dust particles compared to the non-Saharan dust aerosol particles. For low particle concentrations close to the detection limit of the nephelometer and aethalometer, the hourly values of the SSA and hence  $\alpha_{\text{SSA}}$  become very noisy, and thus the criterion becomes increasingly uncertain on an hourly base. During CLACE2014, one clear SDE was detected by this method, which lasted for 4.5 h. It was the maximum of a period of about 4 days during which very low Saharan dust concentration was present. A combined approach using the  $\alpha_{\text{SSA}}$ , PM10 mass concentration, particle size distribution, and calculated back trajectories, as well as particle dispersion model output in addition to the strontium isotopic ratio analysis, was applied to determine the presence of dust potentially originating from the Sahara as well as other aerosol sources.

#### 9) AIRMASS ORIGIN MODELING: FLEXPART AND LAGRANTO

A four-dimensional response function (three spatial dimensions plus time), the so-called footprint emission sensitivity, was obtained from the Lagrangian flexible particle dispersion model (FLEXPART) products browser at Empa ([http://lagrange.empa.ch/FLEXPART\\_browser/](http://lagrange.empa.ch/FLEXPART_browser/)) (Stohl et al. 2005; Sturm et al. 2013; Pandey Deolal et al. 2014). FLEXPART simulates the release of 50 000 particles every 3 h and follows them backward in time. The Jungfraujoch at an altitude of 3580 m MSL was chosen as the release location. It is driven by ECMWF Integrated Forecast System wind fields. The footprint emission sensitivity product is integrated over the lowest 100 m above the surface and is proportional to the residence time of the particles over a unit area. It gives an indication where emissions are likely to originate from (for further information, see <http://transport.nilu.no/flexpart/model-information>).

Using the Lagrangian analysis tool LAGRANTO (Wernli and Davies 1997), an ensemble of 10-day back trajectories was calculated for every 6 h. The trajectories end at the position of the Jungfraujoch Sphinx station at a pressure of  $p = 654$  hPa. To best capture random variations and differences in transport with altitude, end points were set additionally to 604, 704, and 754 hPa, as well as to  $0.5^\circ$  north, south, east, and west of the

Jungfraujoch. The pressure at the level of the trajectory and the PBL height were tracked along each trajectory.

### 3. Results and discussion

In the following, the meteorological conditions during the three campaigns are presented (section 3a) and discussed in the context of PBL air influence (section 3b). An overview of the INP concentrations during the three winter periods is given in section 3c. Their correlation to different aerosol species and airmass origins is discussed in section 3d, and the in-cloud versus out-of-cloud INP loading is presented in section 3e. Three case studies from CLACE2014 are analyzed in section 3f. We compare the Jungfraujoch INP data to a large INP dataset from the literature in section 3g. Last, we discuss the effect of overpredicting average INP concentrations by not reporting data below the detection limit in section 3h.

#### a. Meteorological situation at the Jungfraujoch

During the 2012 campaign period, a high pressure system over southern Europe persisted. The Jungfraujoch was right at the edge of this system and continuously influenced by cyclonic activity over north and east Europe, leading to mostly northwesterly winds (91% of the PINC measurement time, as shown in Fig. 3a; mean wind speed during the measurement period:  $10.9 \text{ m s}^{-1}$ ).

The weather pattern during CLACE2013 was very progressive with frontal systems passing frequently. This was interrupted by two stable situations: first, at the end of January, with an Azore high leading to westerly flows, and, second, during mid-February when a high-pressure system developed over Scandinavia. At the very end of CLACE2013, a cold air pool developed, leading to lower temperatures in western Europe. The wind came mainly from the northwest during the first part of the campaign and from the east toward the end (86% of the PINC measurement time, as shown in Fig. 3b; mean wind speed:  $7.7 \text{ m s}^{-1}$ ).

During CLACE2014, low pressure systems frequently passed Jungfraujoch. A persistent high pressure system over eastern Europe led to a blocking situation. Strong southeasterly winds occurred (mean wind speed:  $10.1 \text{ m s}^{-1}$ ), which were often associated with foehn events. Only 45% of the PINC measurements were obtained in northwest wind situations during CLACE2014 (see Fig. 3c). The PINC measurement time in clouds was 55% during CLACE2013 and 68% during CLACE2014 (section 3e). No cloud event times are available for the 2012 measurement period because the PVM-100 was not installed. Ambient temperatures

during the 2012 measurement period were, in general, higher ( $\bar{T} = 260 \text{ K}$ ) than during the later campaigns (256 K in 2013 and 258 K in 2014; Fig. 3d). During CLACE2014, Saharan dust was advected over Switzerland between 31 January and 2 February 2014. This was confirmed by different methods and is discussed in section 3f. No Saharan dust was detected during the 2012 and 2013 measurements with our methods described in section 2d.

#### b. Free-tropospheric conditions

According to earlier studies, 60%–68% of the time during winter the Jungfraujoch is exposed to free-tropospheric conditions (Zellweger et al. 2003; Herrmann et al. 2015). For the current study, the ratio of  $\text{NO}_y$  to CO was used as a tracer of PBL air influence or local emissions, as suggested by Zellweger et al. (2003). Close to anthropogenic sources,  $\text{NO}_y/\text{CO}$  is about 0.1 and values of about 0.005 are typical for the free troposphere (Jaeglé et al. 1998). Pandey Deolal et al. (2013) compared the  $\text{NO}_y/\text{CO}$  ratio to other tracer-tracer ratios. They suggested a  $\text{NO}_y/\text{CO}$  ratio of 0.008 to distinguish between free-tropospheric and locally influenced air at the Jungfraujoch. For an additional, independent airmass characterization, we also analyzed back trajectories with respect to their residence time in the PBL during the last 10 days before reaching the Jungfraujoch. The  $\text{NO}_y/\text{CO}$  and back trajectory methods agreed about 75% of the time during CLACE2014 when using the 0.005 threshold. During CLACE2014, 21% of the INP measurements were conducted when  $\text{NO}_y/\text{CO}$  values below 0.005 were observed and 64% below 0.008. During the three periods, the maximum  $\text{NO}_y/\text{CO}$  ratio was 0.03 during CLACE2014, which shows that pollution from tourism and construction work at the Jungfraujoch was negligible. The EBC mass concentration was examined as an indicator of the effect of PBL-influenced air masses or local pollution on the aerosol loading. Peaks in the EBC concentration usually correspond to times of higher  $\text{NO}_y/\text{CO}$ . The  $\text{NO}_y/\text{CO}$  ratio was mostly below 0.005 during the measurement periods in 2012 (88%) and 2013 (80%) (i.e., the conditions were mostly free tropospheric). During the measurement period in 2012, the lowest EBC concentration was observed (campaign median:  $7.3 \text{ ng m}^{-3}$ ); CLACE2013 and CLACE2014 were slightly more polluted (campaign median: 16.55 and  $14.4 \text{ ng m}^{-3}$ , respectively). In conclusion, the CLACE2014 measurements seem to have been more often affected by PBL air than the other measurement periods, but the pollution level, which may affect ice nucleation, was similarly low compared to that during the clearly free-tropospheric periods.

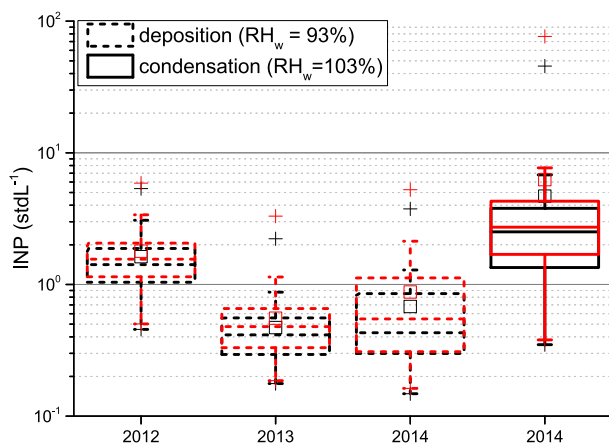


FIG. 4. Averaged INP concentration at  $T = 241$  K in deposition ( $RH_w = 93\%$ , dashed line) and condensation ( $RH_w = 103\%$ , solid line) mode. See the caption of Fig. 3 for box-plot details. In black are the measured INP concentrations; red includes the assumed INP too large to be sampled by PINC.

### c. Ice nucleating particle concentration

Figure 4 shows the median (middle bars) and mean (squares) INP concentrations measured. This analysis excludes data that fell below the limit of detection. The INP concentrations as measured in PINC are in black; those including the omitted INP are in red. In January 2012, generally higher INP concentrations were detected than during CLACE2013 and 2014, when INP concentrations were similarly low. The general decrease of the averaged data during CLACE2013 and 2014 compared to 2012 is mostly related to the use of the concentrator and the lowered LOD. This means for the 2013 and 2014 campaign averages, we were able to include lower sampled concentrations that were left out of the 2012 campaign average because of the higher LOD in 2012. The highest INP concentrations during the campaigns in 2013 and 2014 are also lower than those of 2012 and unrelated to the LOD. In 2014, the condensation mode INP concentration is, on average, one order of magnitude higher than in deposition mode. It spans from less than  $1 \text{ stdL}^{-1}$ , which is comparable to concentrations found in deposition mode, up to  $45.6 (77.0) \text{ stdL}^{-1}$ .

In Fig. 5, 20-min averaged INP concentrations are shown. When INP concentrations fell below the LOD, a gray drop line expresses the range they lie within. The upper limit of a drop line is equal to the LOD, which changes depending on the quality of the corresponding background measurements. The decrease of the LOD due to the use of the concentrator is seen by shorter drop lines in Figs. 5b and 5c compared to Fig. 5a. All three plots show INP concentrations in the deposition regime ( $RH_w = 93\%$ ). Only small variations can be seen for each

of the three measurement periods. INP concentrations range from  $0.46$  to  $5.35 \text{ stdL}^{-1}$  (corrected: from  $0.50$  to  $5.9 \text{ stdL}^{-1}$ ) in 2012, from  $0.18$  to  $2.23 \text{ stdL}^{-1}$  (from  $0.2$  to  $3.3 \text{ stdL}^{-1}$ ) in 2013, and from  $0.15$  to  $3.8 \text{ stdL}^{-1}$  (from  $0.2$  to  $5.2 \text{ stdL}^{-1}$ ) in 2014 in the deposition regime. During CLACE2014, usually INP concentrations of  $0.4$ – $10 \text{ stdL}^{-1}$  were detected in the condensation regime, where almost all data points are above the LOD; thus, there are hardly any drop lines in Fig. 5d. However, in the evening of 16 February 2014, a strong increase in the condensation INP concentration to up to  $45.6 \text{ stdL}^{-1}$  ( $77.0 \text{ stdL}^{-1}$ ) was observed, which is discussed in section 3f.

### d. Role of different ambient aerosol species as INP

#### 1) BIOLOGICAL PARTICLES

Some biological particles are known to nucleate ice even at temperatures warmer than  $263$  K (Diehl et al. 2001; Després et al. 2012; Hoose and Möhler 2012). Table 3 shows an overview of the ratios of fluorescent and non-fluorescent particles to total particle concentrations larger than  $0.8 \mu\text{m}$  as measured by the WIBS during CLACE2014. Furthermore, the fluorescent particles were subdivided into three clusters based on their fluorescent signals. Clusters C1 and C2 are weakly fluorescent, representative of mineral dust aerosol (Pöhlker et al. 2012). Cluster C3 is moderately fluorescent, and particles are likely of biological origin (Crawford et al. 2014). Table 3 shows that the majority of particles were nonfluorescent (74%) during the CLACE2014 PINC measurement time. Almost all of the fluorescent particles were C2 particles (i.e., likely mineral dust). Only a negligible fraction was classified as biological (median = 0; mean = 0.005). Of these particles, none was found in the size range of particles that could enter PINC ( $0.8$ – $1 \mu\text{m}$ ). Thus, biological particles did not play a role for ice nucleation at Jungfraujoch during these wintertime measurement periods (see also Crawford et al. 2016).

The condensation  $\text{INP}_{241\text{K},103\%}$  correlated well with the concentration of nonfluorescent particles ( $R^2 = 0.90$ ) of a size of  $0.8$ – $1 \mu\text{m}$ . No correlation was found with fluorescent particles from all three clusters and of the same size, suggesting that the cause of the weak fluorescence does not influence the ice nucleation activity. For deposition INPs, no correlation was found with total particle concentration in this size range which is in agreement with the observation that the deposition INP concentrations were very low and showed no temporal variability.

#### 2) BLACK CARBON

EBC mass concentration correlated very weakly with condensation  $\text{INP}_{241\text{K},103\%}$  ( $R^2 = 0.11$ ) and not at all

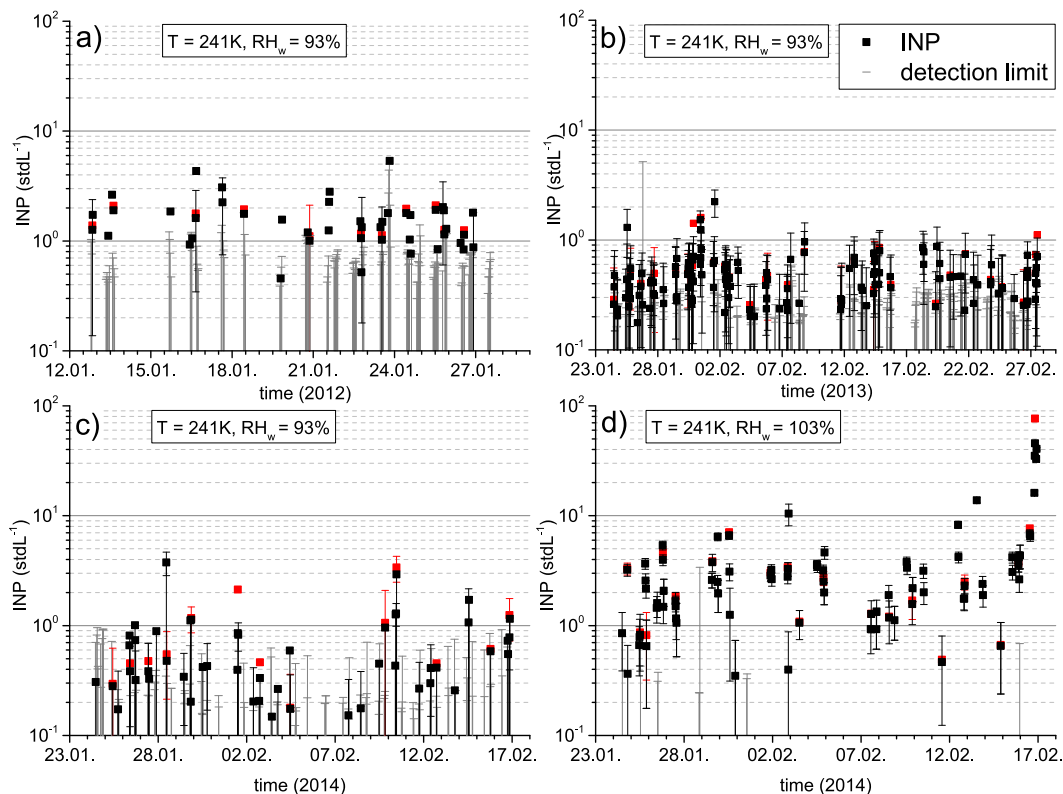


FIG. 5. Time series of 20-min averages of INP concentration at  $T = 241$  K in deposition mode ( $RH_w = 93\%$ ) in (a) January 2012, (b) January and February 2013, (c) January and February 2014, and (d) condensation mode ( $RH_w = 103\%$ ) during January and February 2014. Gray drop lines indicate the detection limit in cases when the INP concentration  $\leq$  LOD. Black squares represent data that are above the detection limit. Error bars are given only for a random subset for visual clarity. The red data indicate the corrected INP concentrations, for which also only a random subset is shown.

with that in deposition mode  $INP_{241K,93\%}$  (negative  $R^2$ ) during CLACE2014. A similar trend is seen also for the campaign averages. About 3-times-higher deposition  $INP_{241K,93\%}$  were found in January 2012 when EBC was the lowest. The  $INP_{241K,93\%}$  were comparably low during CLACE2013 and 2014, even though EBC concentrations were similar to 2012 levels, and the  $NO_y/CO$  indicated more PBL air influence during CLACE2014. This is in agreement with earlier observations by Chou et al. (2011) for  $INP_{241K,93\%}$ . Kamphus et al. (2010) also did not find EBC to be enriched in ice crystal residuals compared to the ambient aerosol. However, this is in contrast to Cozic et al. (2008), who found enrichment of EBC in ice crystal residuals, and to Targino et al. (2009), who observed an enhancement of the ice phase in clouds at the Jungfraujoch during times of elevated pollution.

### 3) SAHARAN DUST

The  $PM_{10}$  concentration was below  $7 \mu g m^{-3}$  throughout CLACE2014 and also during the SDE in early February 2014. Conen et al. (2015) classified periods of

$PM_{10} < 10 \mu g m^{-3}$  at the Jungfraujoch as periods without Saharan influence. This shows that the detected SDE (see section 2d) was comparably weak in terms of dust particle mass concentration. Our measurements below water saturation at  $T = 247$  K,  $INP_{247K,93\%}$ , and  $INP_{247K,98\%}$  revealed that this weak SDE had no effect on the deposition INP concentration at this temperature. A small increase of a factor of 2 compared to the campaign average was observed for deposition  $INP_{241K,93\%}$ . Chou et al. (2011) saw an increase of  $INP_{241K,93\%}$  at these

TABLE 3. Median ratio of (non)fluorescent particles to total particles as measured with the WIBS.

	0.8–1 $\mu m$		0.8–20 $\mu m$	
	Median	Std dev	Median	Std dev
Nonfluorescent	0.81	0.17	0.74	0.14
Fluorescent	0.19	0.17	0.26	0.14
C1	0	0.01	0.05	0.05
C2	0.19	0.17	0.19	0.11
C3	0	0.001	0	0.01

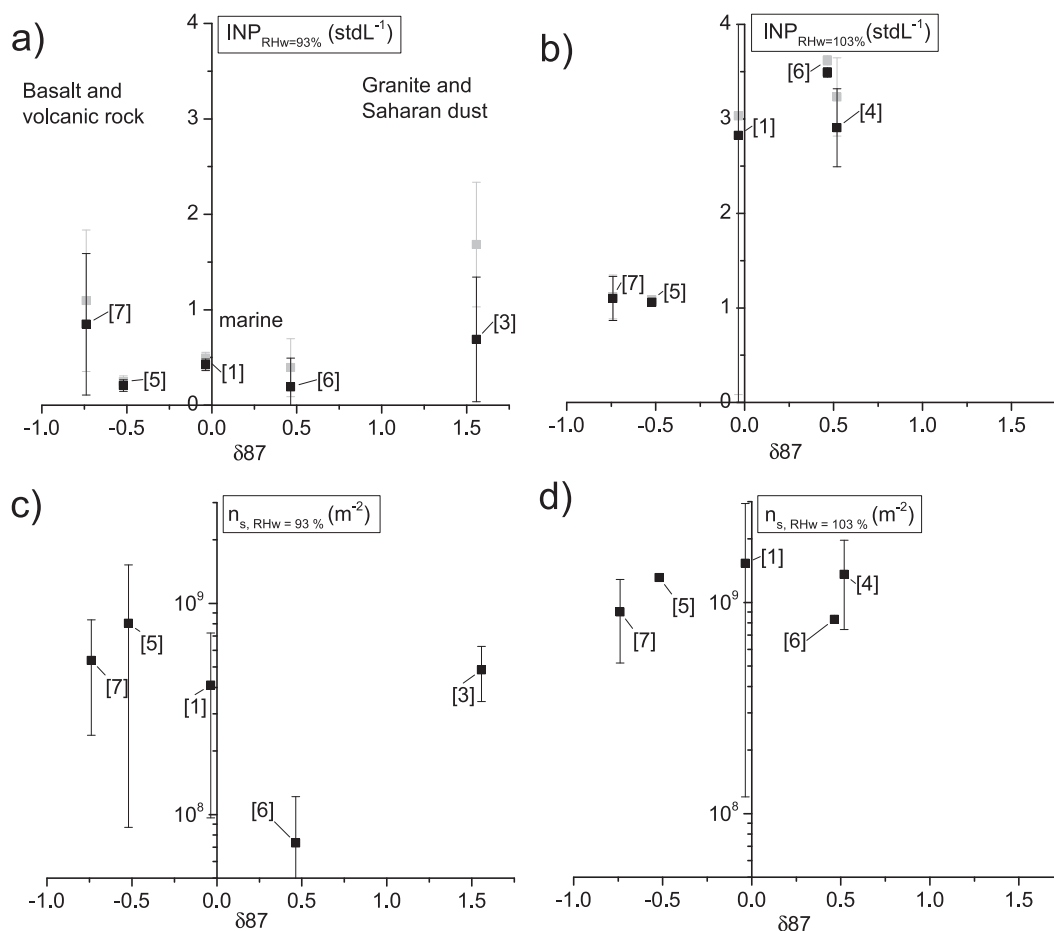


FIG. 6. INP concentration at  $T = 241$  K in (a) deposition ( $RH_w = 93\%$ ) and (b) condensation mode ( $RH_w = 103\%$ ) and  $\delta 87$  from the cloud samples taken in parallel to INP measurements. (c), (d) The ice-active surface site density  $n_s$  in both modes is shown. The combined cloud water sample (Sr sample) numbers are in brackets, and their time of collection can be found in Table A1. Error bars represent the standard deviation of the INP measurements during the period of each cloud sample. In (a) and (b), the corrected INP concentrations are indicated in gray.

chamber conditions by a factor of 2–20 during an SDE in June 2009. The smaller increase in  $INP_{241K,93\%}$  during CLACE2014 SDE likely stems from the lower concentrations of dust particles, which also led to the  $\alpha_{SSA}$  SDE criteria not being met during most of the SDE. Chou et al. (2011) found an increase from less than  $1 \times 10^{-11}$  to over  $20 \times 10^{-11}$  meters per standard cubic centimeters ( $\text{m}^2 \text{std cm}^{-3}$ ) in total aerosol surface area during a SDE, whereas during CLACE2014 the maximum total surface area was  $1.8 \times 10^{-11}$  and  $0.6 \times 10^{-11} \text{m}^2 \text{std cm}^{-3}$  during the small SDE.

#### 4) MARINE AEROSOL VERSUS BASALTIC AND SAHARAN DUST

In Fig. 6, deposition  $INP_{241K,93\%}$  (Fig. 6a) and condensation  $INP_{241K,103\%}$  (Fig. 6b) are compared to the  $\delta 87$  measured in-cloud samples that were collected

during the time of the INP measurements. The positive  $\delta 87$  of samples 4 and 6 indicate that the samples contained a mixture of marine and granitoid or Saharan dust aerosol. Sample 3 contained a substantial amount of Saharan dust, as indicated by its very high, positive  $\delta 87$  value and low Na/Al value compared to the other samples (Fig. A1 in appendix). Sample 1 had a  $\delta 87$  value close to zero and a maximal Na/Al value (see Fig. A1), indicating that this sample was dominated by marine aerosol. The marine aerosol particles are likely composed of sea salt and a nonfluorescent organic fraction (Parlanti et al. 2000; Stedmon et al. 2003), because the concentration of fluorescent biological aerosol particles was very low and given the long transport times from the marine source to the Jungfraujoch. Samples 5 and 7 were influenced by aerosols arising from basaltic or volcanic bedrock (negative  $\delta 87$ ). These findings are supported by

TABLE 4. Median particle concentration CN and total surface area  $A$ , INP concentrations, and ice-active surface site density at  $T = 241$  K in deposition ( $\text{RH}_w = 93\%$ ) and condensation ( $\text{RH}_w = 103\%$ ) for cloudy and cloud-free conditions during CLACE2014. Corrected INP concentrations are given in parentheses. The size ranges in the CN and  $A$  columns are  $d_p = 0.01\text{--}3$  and  $0.02\text{--}20$   $\mu\text{m}$ , respectively.

	CN (std $\text{cm}^{-3}$ )	$A$ ( $\text{m}^2$ std $\text{cm}^{-3}$ )	Deposition INP (stdL $^{-1}$ )	Condensation INP (stdL $^{-1}$ )	Deposition $n_s$ ( $\text{m}^{-2}$ )	Condensation $n_s$ ( $\text{m}^{-2}$ )
In cloud	229	$3.0 \times 10^{-12}$	0.43 (0.57)	2.57 (3.07)	$2.55 \times 10^8$	$1.37 \times 10^9$
Out of cloud	445	$2.5 \times 10^{-12}$	0.44 (0.50)	2.25 (2.38)	$3.07 \times 10^8$	$8.09 \times 10^8$

airmass back trajectory analysis. As the  $^{87}\text{Sr}/^{86}\text{Sr}$  values observed for samples 5 and 7 are higher than those typically found for basaltic rock (Faure 1986), we suggest that these samples represent a mixture of marine and basaltic aerosols.

In the deposition mode (Fig. 6a) no clear differences were found between the  $\text{INP}_{241\text{K},93\%}$  of the basaltic, marine, and Saharan samples. Only when taking the omitted INP into account, the Saharan sample 3 showed a factor-of-3-higher  $\text{INP}_{241\text{K},93\%}$  than the marine sample 1. Condensation  $\text{INP}_{241\text{K},103\%}$  (Fig. 6b) were, on average, higher for the Saharan–marine samples 4 and 6 than for the basaltic samples 5 and 7 and were similar to the marine sample 1. However, when normalizing the INP data by the total aerosol surface area, the Saharan samples 3 and 6 show a lower  $n_s$  than the basaltic samples 5 and 7 in deposition mode (Figs. 6c,d). In condensation mode at 241 K, all samples have a similar  $n_s$ , with the marine sample 1 being the most ice-active. This is an indication that, with only weak continental sources, ice nucleation in the free troposphere even far away from oceans can be dominated by likely nonviable marine aerosol, similar to the observations by Knopf et al. (2014) for a boundary layer site.

#### e. In and out of clouds, wind direction, and other meteorological parameters

During CLACE2014, 68% of the INP measurements were made during in-cloud conditions. Table 4 summarizes the median aerosol particle and INP concentrations in and out of cloud. There were, on average, a factor of 2 more aerosol particles in the size range of the CPC ( $\geq 0.01$   $\mu\text{m}$ ) during cloud-free periods than during cloudy ones. Yet a larger (20%) total aerosol surface area was found in clouds, indicating that there were more large particles in cloud than out of cloud. This is in line with 14% (corrected: 29%) higher median condensation  $\text{INP}_{241\text{K},103\%}$  in cloud than out of cloud. However, in light of the relatively high uncertainty of the INP concentrations, these results are not significant.

Herrmann et al. (2015) also found higher concentrations of particles below 600 nm out of cloud than in cloud under free-tropospheric conditions in winter. They

attribute this to wet removal processes, as Stopelli et al. (2015) observed that most clouds in winter have precipitated before reaching Jungfraujoch. Whereas Stopelli et al. (2015) showed that INP active at  $T \geq 263$  K are depleted in precipitating clouds at Jungfraujoch, our studies show that the INPs active at  $T = 241$  K (i.e., below ambient temperatures) are not depleted, which is to be expected.

Figure 7 shows INP concentrations from CLACE2013 and CLACE2014 during south wind and north wind conditions. For  $\text{INP}_{241\text{K},93\%}$ , the wind direction does not make a difference in the INP concentration. Above water saturation, there are, on average, about 40% more  $\text{INP}_{241\text{K},103\%}$  found during southeasterly than during northwesterly conditions. Air masses coming from the southeast are more likely to carry dust particles than those from the north (Collaud Coen et al. 2011). This was the case during the CLACE2014 SDE as well as most of the event on 16 February (next section), both of which were periods of increased INP concentrations. Another possible explanation for the difference between north and south winds is that south winds are more often related to foehn events, which can transport PBL air to the Jungfraujoch also in winter. However, since no correlation between the INP concentration and the occurrence of foehn events was found, we conclude that foehn has no effect on INP concentrations at Jungfraujoch.

In contrast to what Conen et al. (2015) found for INPs active at  $T = 265$  K, we did not observe any correlation between INP concentrations at  $T = 241$  K and the ambient temperature, which is likely because of the ambient temperatures being warmer than 241 K. Neither was any correlation found with wind speed or relative humidity.

#### f. Case studies during CLACE2014: Effect of aerosol particle size and source

In this section, three cases are discussed in more detail. We focus on CLACE2014 due to the availability of condensation mode and WIBS data. Figure 8 shows an overview of INP and particle concentrations in different size ranges as well as the concentration of fluorescent particles.

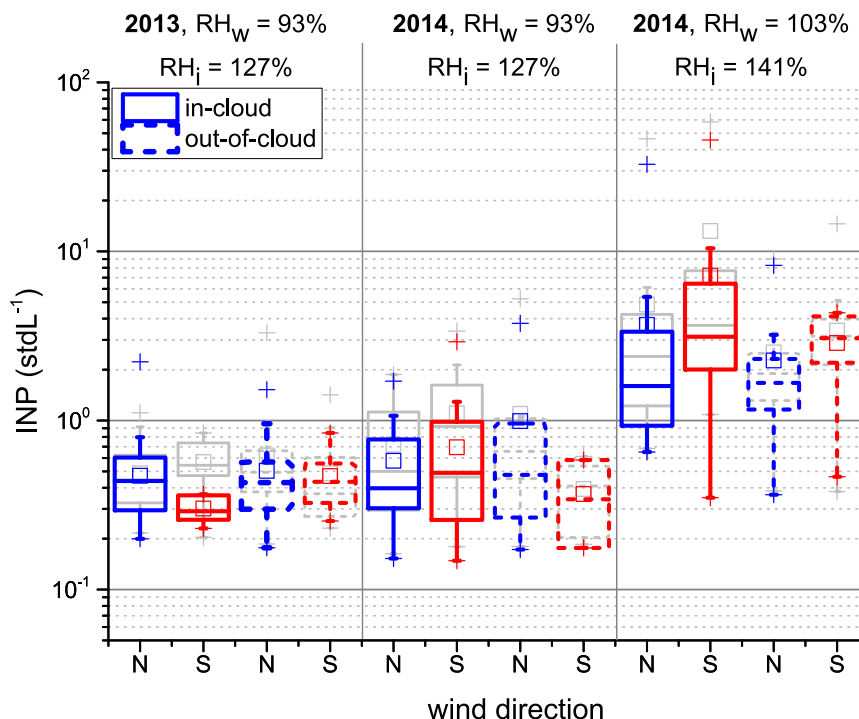


FIG. 7. INP concentration at  $T = 241$  K during in-cloud (solid lines) and out-of-cloud (dashed lines) conditions for north (blue) and south (red) wind situations in 2013 and 2014.  $RH_w$  conditions are indicated on top of the plot. See Fig. 3 for box-plot details. The corrected INP concentrations are indicated in gray.

### 1) CASE 1

From 0856 to 1337 local time (LT) 2 February 2014, an SDE was detected based on the  $\alpha_{SSA}$  criterion (see section 2c). The SDE is also evidenced by the increase in the concentration of particles with diameters between 0.5 and  $1 \mu\text{m}$  and between 0.8 and  $20 \mu\text{m}$ , as shown in Fig. 8d. The aerosol size distribution shows that larger particles such as dust were also present on 1 February and in the evening of 2 February 2014. Isotope samples 2, 3, 4, and 6 show a positive  $\delta 87$  value, pointing to granite or Saharan dust as the main aerosol species, with a distinct maximum for sample 3 on 1 February (Fig. 6a). From 1200 LT 31 January until 1800 LT 4 February, some of the back trajectories indicate that the air masses reaching the Jungfraujoch at the beginning of February passed close to the ground in the Sahara. On 1 February, this is the case for most of the trajectories, as shown in Fig. 9a. Footprint emission sensitivities from the FLEXPART model also indicate Saharan influence from 31 January through 2 February 2014 (Fig. 9d). This demonstrates that the air masses may have carried Saharan dust even during times when the  $\alpha_{SSA}$  criterion was not met and PM10 values were low.

During this comparably weak SDE, INP measurements at  $T = 247$  K and  $RH_w = 93\%$  and at  $RH_w = 98\%$

showed no increase in INP concentration compared to the rest of the measurement period, implying that the dust particles entering PINC were not ice active at these conditions and either required higher RH or lower  $T$  to form ice. At  $T = 241$  K, an increase to  $0.85$  ( $2.1$ )  $\text{stdL}^{-1}$  above the campaign median  $\text{INP}_{241\text{K},93\%}$  concentrations of  $0.43$  ( $0.55$ )  $\text{stdL}^{-1}$  (see Fig. 8a) was observed at 1200 LT 1 February, when an increased concentration of larger particles was present. Only one measurement in the condensation mode  $\text{INP}_{241\text{K},103\%}$  of  $10.4$  ( $14.6$ )  $\text{stdL}^{-1}$  coincided with increased concentrations of large particles during the evening of 2 February. This indicates that the dust particles activated at these conditions, even though the signal is weak both in the deposition and condensation regime.

### 2) CASE 2

An event of elevated  $\text{INP}_{241\text{K},93\%}$  concentrations of  $2.9$  ( $3.4$ )  $\text{stdL}^{-1}$  occurred from 1000 to 1130 LT 10 February 2014 (Fig. 8a). This corresponds to the tail of an event of increased aerosol concentrations at sizes of several microns, which started the night before and is visible in the OPC data (Fig. 8d) and in the WIBS total and fluorescent aerosol particle concentrations (Fig. 8e). The latter finding indicates that a fraction of the particles were fluorescent

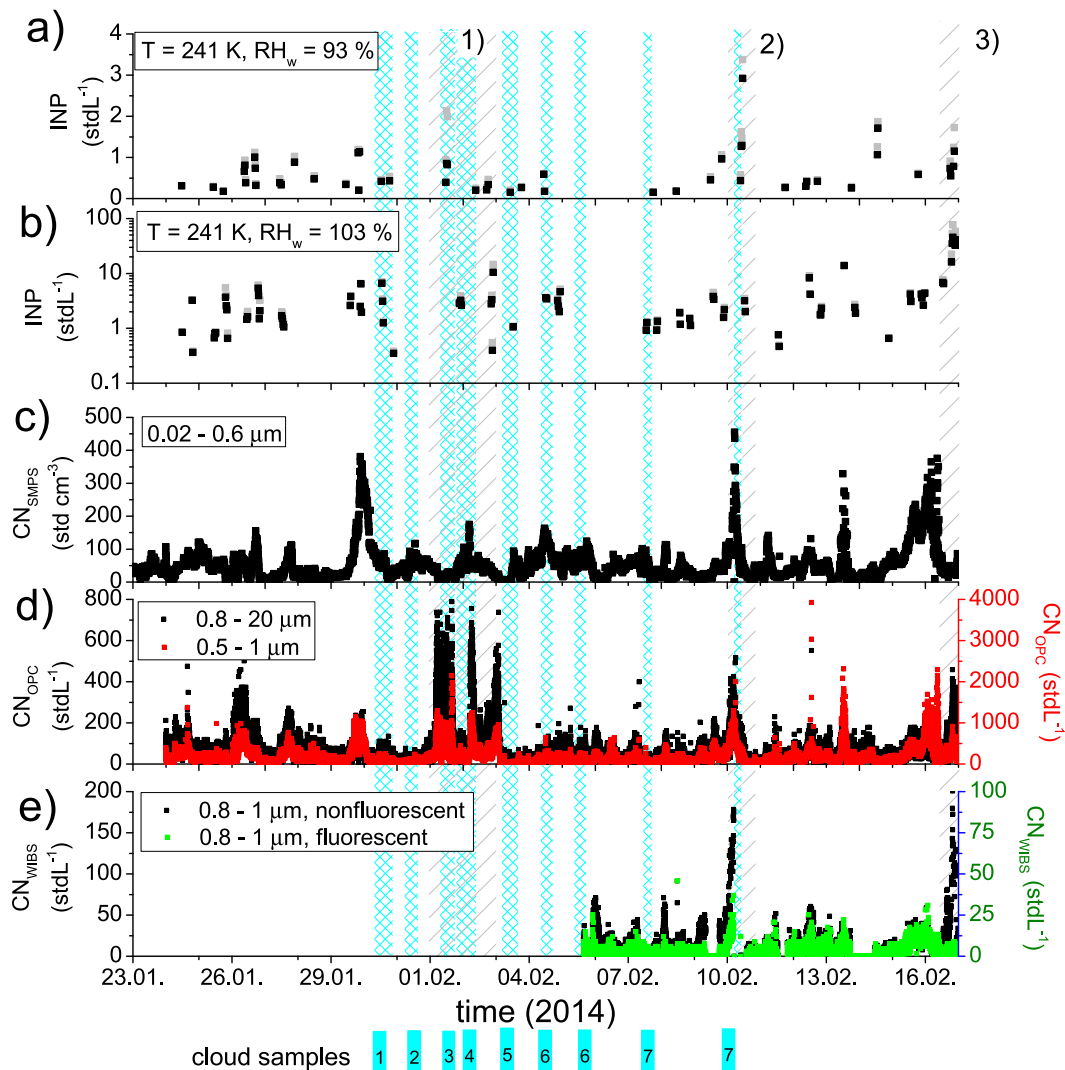


FIG. 8. INP concentration time series during 2014 at  $T = 241$  K in (a) deposition mode ( $RH_w = 93\%$ ) and (b) condensation mode ( $RH_w = 103\%$ ). The corrected INP concentrations are indicated in gray. Concentration of aerosol particles in the size range (c)  $0.02\text{--}0.6\text{-}\mu\text{m}$  mobility diameter as measured by the SMPS and (d)  $0.5\text{--}1\text{-}$  and  $0.8\text{--}20\text{-}\mu\text{m}$  optical diameter measured by the OPC, as well as (e) nonfluorescent and fluorescent particles of  $0.8\text{--}1\text{-}\mu\text{m}$  optical diameter measured by the WIBS. Shaded areas in cyan are times when cloud samples were taken for Sr isotope analysis. Gray shaded areas 1–3 in (a) refer to the three case studies discussed in more detail in [section 3f](#).

mineral dust particles ([section 2d](#)). The presence of dust is further supported by the  $\alpha_{SSA}$  being negative from 0900 to 1000 LT 10 February. Because of a hardware failure, no WIBS data are available for the morning of 10 February. The  $\delta 87$  value was  $-0.74$ , indicating basaltic or volcanic rock as the aerosol origin (see [Fig. 6a](#)). Hence, during this event the increased deposition INP concentration seems to be linked to an increase in the concentration of non-Saharan dust particles. Back trajectories and footprint emission sensitivities from FLEXPART ([Figs. 9b,e](#)) indicate mainly local sources in Switzerland and northern Italy, with potential influence from the Iberian Peninsula.

No measurements at other PINC  $T$  and  $RH$  conditions were conducted during this period.

### 3) CASE 3

On 16 February 2014, a strong increase of condensation  $INP_{241K,103\%}$  to  $45.6$  ( $77.0$ )  $\text{stdL}^{-1}$  was observed ([Fig. 8b](#)). During this time, an increase in the concentration of particles with  $d_p \geq 0.5\text{ }\mu\text{m}$  occurred. The  $\alpha_{SSA}$  SDE criterion was not met. The WIBS measurements show a strong increase in nonfluorescent particle counts but no increase in fluorescent particle numbers. Air masses arriving on that day at 1800 LT

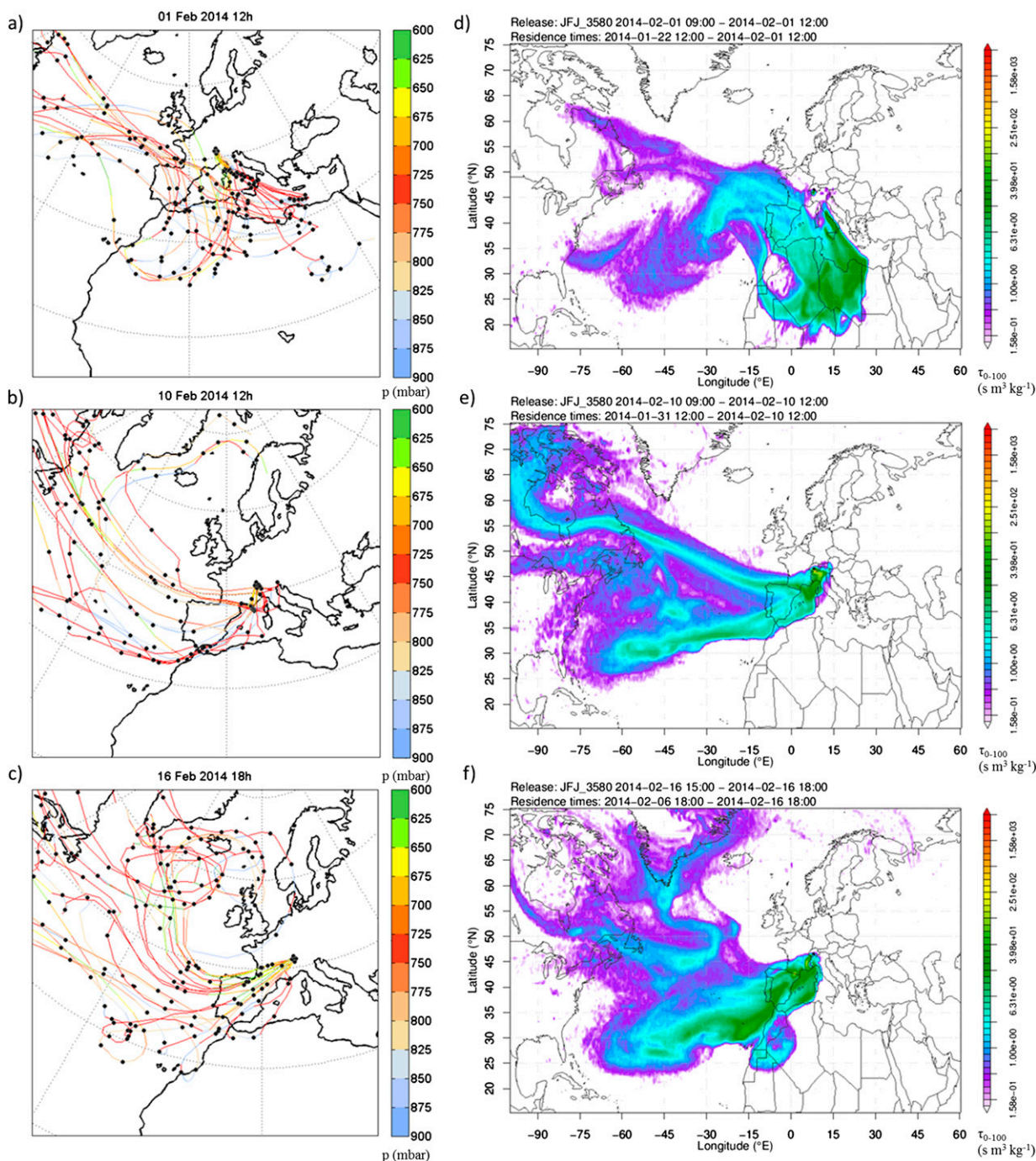


FIG. 9. (a)–(c) 10-day back trajectories calculated with the LAGRANTO model (Wernli and Davies 1997). The color code represents the pressure of the trajectory (hPa). Each 24-h point is represented by a black dot. (d)–(f) FLEXPART emission sensitivity fields (section 2d), integrated from 0 to 100 m above model ground. The color code gives an indication from where a unit volume of emissions is likely to originate.

were mostly influenced by sources on the Iberian Peninsula and from the Atlantic Ocean (see Fig. 9b). FLEXPART confirms these regions as main sources but also indicates a weak source sensitivity for parts of the Sahara. These results suggest that the efficient

condensation  $\text{INP}_{241\text{K},103\%}$  were either mainly of crustal origin with little biological content or potentially large sea spray aerosols, which could not be distinguished in our study because isotope data are not available for this period.

*g. INPs at the Jungfraujoch in comparison to DeMott et al. (2010)*

Figure 10a shows an overview of INP concentrations at relative humidities above water saturation from several field and airborne studies in North America, Brazil, and over the Pacific from DeMott et al. (2010) overlain with the PINC condensation  $\text{INP}_{241\text{K},103\%}$  as well as  $\text{INP}_{241\text{K},98\%}$ . The latter ones were included because water saturation still lies within the RH uncertainty at these conditions. The INP data are the sum of the measured INPs and the calculated omitted INPs that were too large to enter PINC. Figure 10b is also adapted from DeMott et al. (2010) and shows the INP concentration in 3-K temperature bins versus the aerosol particle concentrations of particles larger than  $0.5\ \mu\text{m}$  ( $n_{\text{aer},0.5}$ ) from their comprehensive dataset together with the PINC measurements from CLACE2014. Each constant temperature dataset was fitted with a power law. The gray lines in Fig. 10b show the fits from the original publication, and the magenta line is the fit to the CLACE2014  $\text{INP}_{241\text{K},103\%}$ .

Figure 10a depicts that results from PINC are below the majority of the data points from DeMott et al. (2010) at a given temperature. It shows that the INP loading at the Jungfraujoch, a remote continental site located mainly in the free troposphere during winter, is low compared to other INP datasets. This is likely due to a lower concentration of aerosol particles larger than  $0.5\ \mu\text{m}$  at the Jungfraujoch, as seen in Fig. 10b. The CLACE2014 data points, in magenta, all fall below  $n_{\text{aer},0.5} \leq 1\ \text{std cm}^{-3}$ , whereas they range up to  $20\ \text{std cm}^{-3}$  in DeMott et al. (2010).

The INP concentrations from DeMott et al. (2010) get larger and the power-law fit becomes better with decreasing temperature (from  $R^2 = 0.387$  at 262 K to  $R^2 = 0.5674$  at 240 K). The CLACE2014 INP concentrations also get larger with decreasing temperature, and the correlation with  $n_{\text{aer},0.5}$  improves. At 247 K, no correlation with  $n_{\text{aer},0.5}$  is found, whereas at 241 K  $R^2 = 0.31$ . Despite the lower  $n_{\text{aer},0.5}$ , the particles have been comparably ice active during CLACE2014. The 241-K dataset mostly overlaps with the 240-K dataset from DeMott et al. (2010), which is reasonable given the experimental uncertainties. This is also true for our data at 247 K and DeMott's (2010) data at 246 K.

*h. Data below the detection limit*

In this last section, we address a common problem in experimental work in general but particularly in atmospheric INP measurements in clean environments. In the current study, deposition  $\text{INP}_{241\text{K},93\%}$  were often close to or below the limit of detection, as shown in Fig. 5. This was also true for the measurements presented here at warmer

temperatures. Typically, data falling below instrument detection limits are disregarded (i.e., censored). However, when measuring in the atmosphere, in very clean environments like the Jungfraujoch in winter, INP concentrations often fall below the LOD of most current INP counters. The number of censored data increases if a more conservative confidence interval of 95% or 99% is used as the LOD. The actual INP concentration during the time of the measurement then can be any value between zero and the LOD. We propose that this is still valuable information. If a large number of data points fall below the LOD, the mean INP concentration depends on how and if these data are accounted for. Not including data below the LOD leads to an overestimation of mean INP concentration, as depicted in Fig. 11. In the current dataset, mean INP concentrations not including data below the LOD are up to a factor of 4 higher than those that include them. This overestimation is reduced with a higher signal-to-noise ratio and less data points falling below the LOD. Therefore, the overestimation of the condensation  $\text{INP}_{241\text{K},103\%}$  due to this effect is only 10% (Fig. 11), which is within the uncertainty of the INP measurements. Different methods have been suggested in the literature for similar problems (e.g., Manly 2001; Chandler and Scott 2011). They range from being rather simplistic, for instance setting all data points below the LOD to random values between zero and the LOD, to being more elaborate methods, which assume a certain distribution of the censored data. To evaluate which of the suggested methods applies best for the case of atmospheric INP measurements lies beyond the scope of this paper. Nevertheless, for future publications of ambient INP measurements, we recommend to report the LOD and data points falling below, in addition to the INP concentrations and their uncertainty.

#### 4. Conclusions

In this paper, INP concentration observations in the free troposphere at the Jungfraujoch during the winter-time in 2012–2014 were presented. Concentrations of INP in the deposition nucleation regime,  $\text{INP}_{241\text{K},93\%}$ , were found to be on average  $1.09 \pm 0.78\ \text{stdL}^{-1}$  ( $1.8 \pm 1\ \text{stdL}^{-1}$ ) during January 2012 and  $0.47 \pm 0.26$  and  $0.68 \pm 0.66\ \text{stdL}^{-1}$  ( $0.5 \pm 0.4$  and  $0.9 \pm 0.9\ \text{stdL}^{-1}$ ) during the CLACE2013 and CLACE2014 campaigns, respectively. In the condensation freezing regime,  $\text{INP}_{241\text{K},103\%}$  increased on average by an order of magnitude to  $4.7 \pm 8.3\ \text{stdL}^{-1}$  ( $6.2 \pm 12.9\ \text{stdL}^{-1}$ ) compared to those in the deposition regime during CLACE2014. During the 2013 and 2014 studies, an aerodynamic lens concentrator was applied upstream of the PINC, which enriched particle concentrations by a factor of  $3 \pm 0.6$ . Hence, the signal to

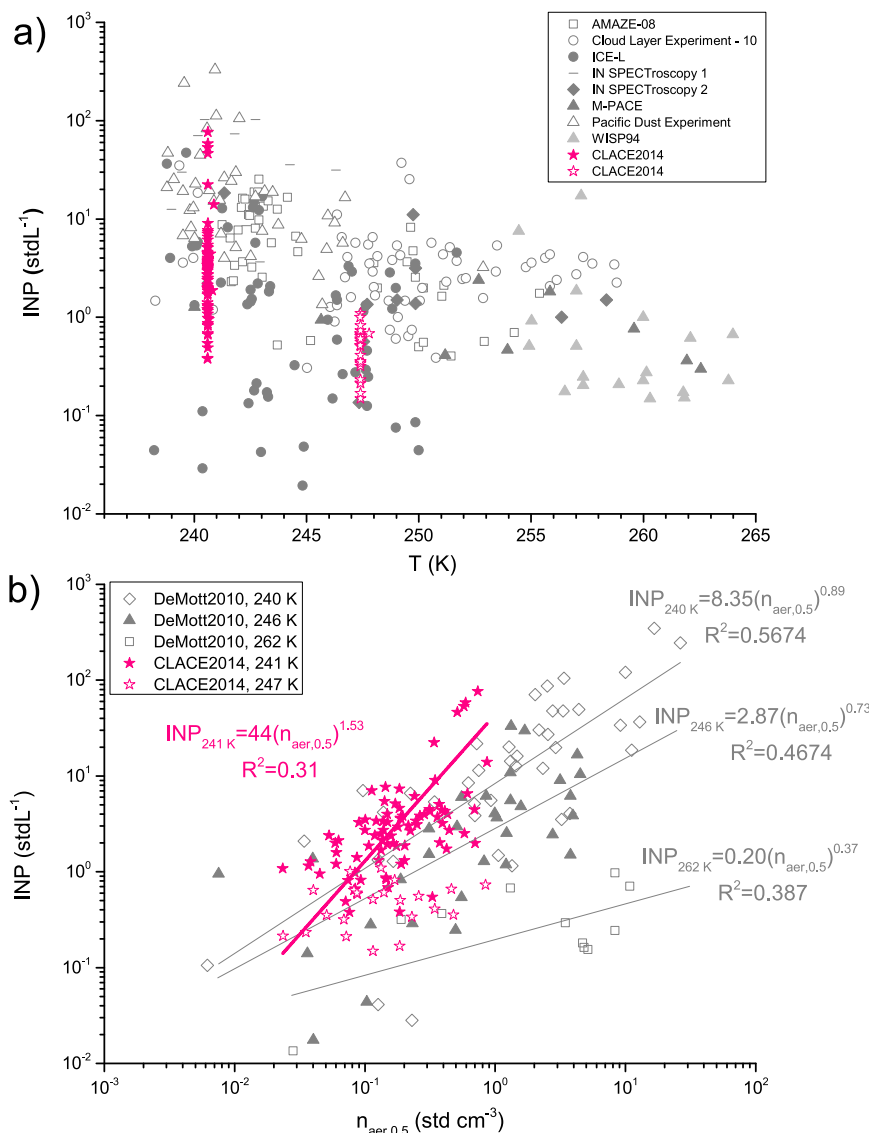


FIG. 10. (a) Corrected INP concentrations as a function of  $T$  at  $RH_w \geq 98\%$  at the Jungfraujoch during CLACE2014 in comparison to those found in several field campaigns in the United States and Brazil and over the Pacific Ocean at  $RH_w \geq 100\%$ . Adapted from DeMott et al. (2010). (b) Same datasets as in (a), but plotted as a function of  $n_{aer,0.5}$  and stratified for 3-K temperature bins. Gray lines are the fits from DeMott et al. (2010); the magenta line is the best fit of the CLACE2014 data at  $T = 241$  K. No fit is presented for the CLACE2014 data at  $T = 247$  K.

noise ratio was increased, which resulted in a lower detection limit for INP concentrations. Compared to earlier studies at several other locations, the observed wintertime, free-tropospheric condensation INP concentrations at the Jungfraujoch are at the lower end. However, normalizing the INP concentrations by the number of aerosol particles larger than  $0.5 \mu\text{m}$  shows that the aerosol particles at the Jungfraujoch are comparably ice active at  $T = 241$  K.

The effects of different types of aerosol particle sources on the INP concentrations were investigated. Deposition  $INP_{241 K, 93\%}$  were similar between CLACE2013, which had lower  $NO_y/CO$  values (free-troposphere air), and CLACE2014, which seems to have been more affected by PBL air. However, EBC concentrations were similarly low during CLACE2013 and CLACE2014 and even lower during the 2012 measurements, when higher INP concentrations were found in

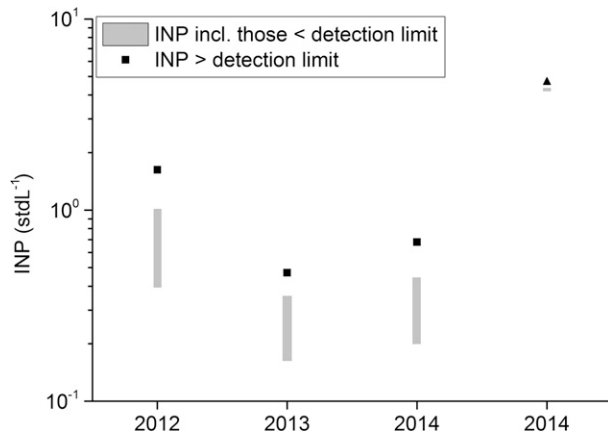


FIG. 11. Mean INP concentration at  $T = 241$  K if data below the detection limit are excluded (deposition mode,  $RH_w = 93\%$ : black squares; condensation mode,  $RH_w = 103\%$ : triangle), set to the value of the detection limit (upper limit of gray shaded area), or set to zero (lower limit of gray shaded area).

deposition mode. Whether periods of lower EBC values are generally related to higher INP concentrations and if the degree of PBL air influence affects INP concentrations are subjects of an ongoing study. Only very low concentrations of biological particles were observed during CLACE2014 and were not found to play a role for ice nucleation during these wintertime measurements. The concentration of fluorescent particles, which were mostly identified as fluorescent mineral dust, were not observed to correlate with the INP concentration, suggesting that the cause of the fluorescence does not affect ice nucleation. A good correlation of non-fluorescent aerosol particles larger than  $0.8 \mu\text{m}$  with condensation  $\text{INP}_{241\text{K},103\%}$  but not with deposition  $\text{INP}_{241\text{K},93\%}$  was found. During 2014, Saharan dust particles led to a small increase of deposition  $\text{INP}_{241\text{K},93\%}$  and condensation  $\text{INP}_{241\text{K},103\%}$  but had no effect on  $\text{INP}_{241\text{K},93\%}$  and  $\text{INP}_{241\text{K},98\%}$ . Evidence for the presence of marine aerosol at the Jungfraujoch was found by strontium isotope analysis of cloud samples ( $\delta 87$  value close to zero) and a maximum in the Na/Al ratio (17.3). As the bioaerosol concentrations were so low, the marine aerosol was likely mostly composed of sea salt as well as some organic fraction, given the transport times from the marine sources to the Jungfraujoch. Aerosol from marine air masses was found to be slightly more ice active at  $T = 241$  K and  $RH_w = 103\%$  in terms of  $n_s$  than that containing Saharan or basaltic dust. However, because of the higher concentrations of particles with  $d_p \geq 0.5 \mu\text{m}$ , absolute INP numbers were higher during the SDE. In January and February 2015, additional cloud samples were collected in parallel to measurements of INP concentrations to be analyzed in a future study.

This should further clarify the influence of air mass origin on particle ice nucleating activity and the role of marine aerosol in comparison to continental sources.

The role of Saharan dust as INP at the Jungfraujoch was further supported by the observation that median condensation INP concentrations were 40% higher during south wind than during north wind conditions, as air masses coming from the south are more likely to transport Saharan dust.

We have shown that reporting ambient INP concentrations below the Poisson statistic-based LOD is important for a more realistic representation of atmospheric INP concentrations. We recommend reporting the LOD as well as data points below the LOD for future studies. When averaging ambient INP measurements, a common method for accounting for data points below the LOD should be agreed on within the atmospheric INP measurement community. To lower the instrumental LOD remains a challenge for current INP counters.

Future measurements at the Jungfraujoch will investigate the seasonal variability of INP concentrations as well as interannual variations. They will be conducted at similar thermodynamic conditions as in the current study. Coupling INP counters, such as PINC, with methods of analyzing the chemical and physical nature of the detected INPs, such as aerosol mass spectrometers, will help us to understand the drivers of ice nucleation in the atmosphere. For long-term observations of atmospheric INPs, a further automation of INP measurement techniques is desirable.

*Acknowledgments.* We thank the three anonymous reviewers for their helpful comments. This work was supported by MeteoSwiss within the Global Atmosphere Watch (GAW) program of the World Meteorological Organization. Y. Boose is funded by the Swiss National Science Foundation (Grant 200020\_150169/1). The research leading to these results has received funding from the European Union's Seventh Framework Programme (FP7/2007-2013) under Grant Agreement 603445 (BACCHUS). The authors thank MeteoSwiss and Jan Henneberger (ETH Zürich) for the meteorological data. We thank Hannes Wydler for his continuous technical assistance with PINC and Fabian Mahrt for the concentrator characterization experiments (ETH Zürich). We express our gratitude to the custodians of the High Altitude Research Station Jungfraujoch, Maria and Urs Otz, as well as Joan and Martin Fischer, for their valuable support. We thank the International Foundation High Altitude Research Station Jungfraujoch and Gornergrat (HFSJG), 3012 Bern, Switzerland for the opportunity to perform experiments at

the Jungfraujoch. We thank Johannes Stählin and Tom Peter (ETH Zürich) for fruitful discussions. Finally, we thank Michael Sprenger, Sara Pousse-Nottelmann, and Christina Schnadt Poberaj (ETH Zürich) for their help with LAGRANTO back trajectory calculations and Stephan Henne (Empa) for the provision of FLEXPART simulations.

## APPENDIX

### Chamber Characterization and Data Treatment

#### *a. Particle losses in the tubing*

Between the total aerosol inlet and the inlet of the PINC chamber, approximately 7 m of 6- and 8-mm inner diameter tubing was installed, in addition to several splits and valves where other instruments were connected. During the CLACE2013 and 2014, a second CPC (TSI, model 3010) was installed right next to the PINC chamber inlet to monitor the aerosol particle concentration. During CLACE2013 the flow in the tubing varied between 11.5 and 12.6 L min<sup>-1</sup>, whereas during CLACE2014 it was 12 L min<sup>-1</sup> during the first week of measurements and 11 L min<sup>-1</sup> for the remaining time after the additional CPC was removed because of a technical failure. The long tubing may have led to significant particle losses. By comparing counts of the CPC right next to the total aerosol inlet to the one right next to the PINC chamber, the total loss of particles between 0.01–3 μm was observed to be on average 25% ± 19% during CLACE2013 and 13% ± 7% during the first week of the CLACE2014 campaign. Similar losses are assumed for the 2012 measurements because of a similar experimental setup as in 2014. However, in the size range, which dominates the ice nucleation in the PINC chamber (0.1–1 μm), fewer losses are expected, as neither Brownian motion nor impaction lead to significant losses here. Therefore, no tubing loss correction is applied to the data.

#### *b. Particle losses in the impactor and PINC chamber*

Upstream of the PINC chamber, an impactor with D<sub>50</sub> = 0.9 μm aerodynamic diameter was used to prevent larger particles entering the chamber and being miscounted as ice crystals. Size-dependent particle losses in the impactor and the chamber itself have been measured with Arizona test dust and montmorillonite, respectively. Losses in the chamber alone were below 5%. For the impactor, size-dependent losses were found (e.g., 50% at 720-nm and 83% at 1000-nm aerodynamic diameter). The data presented here were corrected with a fitted loss curve.

#### *c. PINC chamber characterization*

Validation experiments using sulfuric acid, similar to those described in Chou et al. (2011), were performed between the CLACE2013 and CLACE2014 campaigns. They showed that the temperature and relative humidity conditions in PINC are established correctly at temperatures below 235 K. An uncertainty in temperature of 0.4 K and thus in relative humidity of 4% has been observed similar to Kanji et al. (2013). Chou et al. (2011) also validated the chamber at  $T = 243$  K by observing the deliquescence point of ammonium sulfate and homogeneous freezing of ammonium sulfate droplets at 233 K. Furthermore, PINC participated in two instrument intercomparison studies, which are published in Wex et al. (2015) and Hiranuma et al. (2015). In both studies, PINC results at RH<sub>w</sub> = 105% and at temperatures below  $T = 261$  K were found to compare well to those of other instruments that measured mostly in the immersion mode. At temperatures above  $T = 261$  K, a high-enough supersaturation to compare to the immersion mode measurements of other instruments is not reachable without droplets surviving the evaporation section of PINC and thus being miscounted as ice crystals. However, in deposition and condensation mode, measurements are possible up to  $T = 265$  K and RH<sub>w</sub> = 101%.

#### *d. Cloud sampling and sample handling*

Cloud samples were collected using a Teflon impaction surface that was placed outside, on the Sphinx's lower terrace facing the wind. Supercooled droplets hit the impaction surface and froze into rimed ice. Every few hours, depending on the sample size, the impaction surface with the cloud sample was brought inside, and the sample was scraped into a clean ziplock bag using a plastic spatula. After the rimed ice melted, it was collected into 50-ml vials. The impact ion surface was cleaned between samples by rinsing it with double distilled water (DDW) and superpure nitric acid at a volumetric ratio of ≈1:1000. Once a day, a blank sample was taken by rinsing the sampler with DDW and collecting it into a clean ziplock bag and then transferring it to a 50-mL vial. Details of sampling times, amount collected, samples' Sr concentrations, and daily blank Sr concentrations are provided in Table A1. After collection, the samples were brought to the clean laboratory of the Institute of Earth Sciences at the Hebrew University of Jerusalem. The samples were acidified with 15 mol L<sup>-1</sup> nitric acid in a volume ratio of 1:100 and were analyzed for metal concentrations with an ion coupled plasma mass spectrometer (Agilent 7500cx; Santa Clara, California). ICP-MS calibration was done using blanks (DDW with a volumetric ratio of 1:100 HNO<sub>3</sub>), a series

TABLE A1. Cloud sample times during CLACE2014.

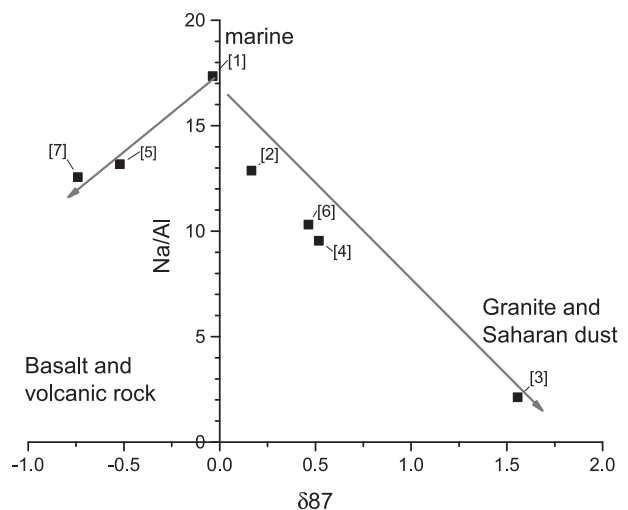
Sample	Start time	End time	Sample volume (mL)	Sr concentration (ppt)	Sr sample
Cloud-01	0915 LT 30 Jan	1215 LT 30 Jan	18	291	1
Cloud-02	1215 LT 30 Jan	1415 LT 30 Jan	16	327	1
Cloud-03	1415 LT 30 Jan	1700 LT 30 Jan	25	581	1
Cloud-04	1700 LT 30 Jan	1915 LT 30 Jan	22	579	1
Cloud-05	1915 LT 30 Jan	2300 LT 30 Jan	18	294	1
Blank140131	31 Jan		45	54	
Cloud-06	0530 LT 31 Jan	0730 LT 31 Jan	12	699	2
Cloud-07	0730 LT 31 Jan	0930 LT 31 Jan	13	323	2
Cloud-08	0930 LT 31 Jan	1130 LT 31 Jan	19	234	2
Cloud-09	1130 LT 31 Jan	1430 LT 31 Jan	45	312	2
Cloud-10	1430 LT 31 Jan	1800 LT 31 Jan	27	689	2
Blank140201	1 Feb		50	58	
Cloud-11	0945 LT 1 Feb	1230 LT 1 Feb	37	3832	3
Cloud-12	1230 LT 1 Feb	1630 LT 1 Feb	7	5348	3
Cloud-13	1630 LT 1 Feb	2100 LT 1 Feb	69	565	3
Cloud-14	2100 LT 1 Feb	2315 LT 1 Feb	36	526	4
Cloud-15	2315 LT 1 Feb	0530 LT 2 Feb	12	877	4
Blank140203	3 Feb		52	99	
Cloud-16	0800 LT 3 Feb	1215 LT 3 Feb	148	172	5
Cloud-17	0915 LT 3 Feb	1215 LT 3 Feb	51	534	5
Cloud-18	0915 LT 3 Feb	1215 LT 3 Feb	34	2272	5
Cloud-19	0915 LT 3 Feb	1215 LT 3 Feb	103	205	5
Blank140204	4 Feb		48	60	
Cloud-20	0915 LT 4 Feb	1215 LT 4 Feb	28	746	6
Blank140205	5 Feb		50	77	
Cloud-21	0915 LT 5 Feb	1215 LT 5 Feb	28	315	6
Blank140207	7 Feb		50	70	
Cloud-23	0900 LT 7 Feb	1300 LT 7 Feb	10	623	7
Cloud-24	1300 LT 7 Feb	1730 LT 7 Feb	54	227	7

of multielement standard solutions ( $1 \text{ ng L}^{-1}$ – $100 \mu\text{g L}^{-1}$  Merck multielement VI), and major elements standards ( $300 \mu\text{g L}^{-1}$ – $3 \text{ mg L}^{-1}$ ). For drift correction, a solution of internal standards was injected with the sample input ( $50 \mu\text{g L}^{-1}$  Sc,  $5 \mu\text{g L}^{-1}$  Re and Rh). The precision was examined using standard reference samples (USGS SRS T-199 and T-207), and accuracy was assessed by repeating the measurements of several samples. Analytical detection limit, precision, and accuracy values of the relevant elements for this paper (Na, Al, and Sr) are provided in Table A2. The isotopic ratio of Sr ( $^{87}\text{Sr}/^{86}\text{Sr}$ ) was measured using the multicollector inductively coupled plasma mass spectrometer (Neptune Plus) (Fig. A1 shows the  $\delta 87$  parameter vs. the Na/Al ratio, a commonly used tracer for marine aerosol. A smaller Na/Al ratio corresponds to a higher absolute  $\delta 87$ , i.e., less marine air.) To

separate the Sr from the sample, we used Sr-Spec resin and followed the method described in Stein et al. (1997). A strontium carbonate isotopic standard [National Institute of Standards and Technology (NIST) SRM 987]

TABLE A2. Cloud sample analysis quality.

Element	Mean precision	Mean accuracy	Detection limit
Na	1%	92%	10 ppb
Al	2%	96%	0.03 ppb
Sr	1%	99%	10 ppt

FIG. A1. Na/Al ratio vs  $\delta 87$ , indicating the geochemical origin of the aerosol. Times of the specific samples can be found in Table A1.

was measured every three samples and had a mean value of  $0.71024 \pm 0.00001$  ( $1\sigma$ ,  $n = 4$ ). The ( $^{87}\text{Sr}/^{86}\text{Sr}$ ) values were corrected for mass fractionation to  $^{86}\text{Sr}/^{84}\text{Sr} = 0.1194$ .

## REFERENCES

- Appenzeller, C., M. Begert, E. Zenklusen, and S. C. Scherrer, 2008: Monitoring climate at Jungfraujoch in the high Swiss Alpine region. *Sci. Total Environ.*, **391**, 262–268, doi:10.1016/j.scitotenv.2007.10.005.
- Archuleta, C., P. DeMott, and S. Kreidenweis, 2005: Ice nucleation by surrogates for atmospheric mineral dust and mineral dust/sulfate particles at cirrus temperatures. *Atmos. Chem. Phys.*, **5**, 2617–2634, doi:10.5194/acp-5-2617-2005.
- Ardon-Dryer, K., and Z. Levin, 2014: Ground-based measurements of immersion freezing in the eastern Mediterranean. *Atmos. Chem. Phys.*, **14**, 5217–5231, doi:10.5194/acp-14-5217-2014.
- Atkinson, J., and Coauthors, 2013: The importance of feldspar for ice nucleation by mineral dust in mixed-phase clouds. *Nature*, **498**, 355–358, doi:10.1038/nature12278.
- Attard, E., H. Yang, A.-M. Delort, P. Amato, U. Pöschl, C. Glauz, T. Koop, and C. E. Morris, 2012: Effects of atmospheric conditions on ice nucleation activity of *Pseudomonas*. *Atmos. Chem. Phys.*, **12**, 10 667–10 677, doi:10.5194/acp-12-10667-2012.
- Avramov, A., and Coauthors, 2011: Toward ice formation closure in Arctic mixed-phase boundary layer clouds during ISDAC. *J. Geophys. Res.*, **116**, D00T08, doi:10.1029/2011JD015910.
- Baltensperger, U., H. W. Gäggeler, D. T. Jost, M. Lugauer, M. Schwikowski, and E. Weingartner, 1997: Aerosol climatology at the high-alpine site Jungfraujoch, Switzerland. *J. Geophys. Res.*, **102**, 19 707–19 715, doi:10.1029/97JD00928.
- Bigg, E., 1967: Cross sections of ice nucleus concentrations at altitude over long paths. *J. Atmos. Sci.*, **24**, 226–229, doi:10.1175/1520-0469(1967)024<0226:CSOINC>2.0.CO;2.
- , 1973: Ice nucleus concentrations in remote areas. *J. Atmos. Sci.*, **30**, 1153–1157, doi:10.1175/1520-0469(1973)030<1153:INCIRA>2.0.CO;2.
- Boucher, O., and Coauthors, 2013: Clouds and aerosols. *Climate Change 2013: The Physical Science Basis*, T. F. Stocker, et al., Eds., Cambridge University Press, 571–657. [Available online at [http://www.climatechange2013.org/images/report/WG1AR5\\_Chapter07\\_FINAL.pdf](http://www.climatechange2013.org/images/report/WG1AR5_Chapter07_FINAL.pdf).]
- Bukowiecki, N., and Coauthors, 2016: A review of more than 20 years of aerosol observation at the high altitude research station Jungfraujoch, Switzerland (3580 m asl). *Aerosol Air Qual. Res.*, **16**, 764–788, doi:10.4209/aaqr.2015.05.0305.
- Capo, R. C., B. W. Stewart, and O. A. Chadwick, 1998: Strontium isotopes as tracers of ecosystem processes: Theory and methods. *Geoderma*, **82**, 197–225, doi:10.1016/S0016-7061(97)00102-X.
- Castro, A., J. L. Marcos, J. Dessens, J. L. Sánchez, and R. Fraile, 1998: Concentration of ice nuclei in continental and maritime air masses in León (Spain). *Atmos. Res.*, **47–48**, 155–167, doi:10.1016/S0169-8095(98)00060-X.
- Chandler, R., and E. M. Scott, 2011: *Statistical Methods for Trend Detection and Analysis in the Environmental Sciences*. John Wiley & Sons, Ltd., 388 pp.
- Chernoff, D. I., and A. K. Bertram, 2010: Effects of sulfate coatings on the ice nucleation properties of a biological ice nucleus and several types of minerals. *J. Geophys. Res.*, **115**, D20205, doi:10.1029/2010JD014254.
- Chou, C., O. Stetzer, E. Weingartner, Z. Jurányi, Z. A. Kanji, and U. Lohmann, 2011: Ice nuclei properties within a Saharan dust event at the Jungfraujoch in the Swiss Alps. *Atmos. Chem. Phys.*, **11**, 4725–4738, doi:10.5194/acp-11-4725-2011.
- , and Coauthors, 2013: Effect of photochemical ageing on the ice nucleation properties of diesel and wood burning particles. *Atmos. Chem. Phys.*, **13**, 761–772, doi:10.5194/acp-13-761-2013.
- Collaud Coen, M., E. Weingartner, D. Schaub, C. Hueglin, C. Corrigan, S. Henning, M. Schwikowski, and U. Baltensperger, 2004: Saharan dust events at the Jungfraujoch: Detection by wavelength dependence of the single scattering albedo and first climatology analysis. *Atmos. Chem. Phys.*, **4**, 2465–2480, doi:10.5194/acp-4-2465-2004.
- , —, M. Furger, S. Nyeki, A. S. H. Prévôt, M. Steinbacher, and U. Baltensperger, 2011: Aerosol climatology and planetary boundary influence at the Jungfraujoch analyzed by synoptic weather types. *Atmos. Chem. Phys.*, **11**, 5931–5944, doi:10.5194/acp-11-5931-2011.
- Conen, F., S. Henne, C. Morris, and C. Alewell, 2012: Atmospheric ice nucleators active  $\geq -12^\circ\text{C}$  can be quantified on  $\text{PM}_{10}$  filters. *Atmos. Meas. Tech.*, **5**, 321–327, doi:10.5194/amt-5-321-2012.
- , S. Rodríguez, C. Hüglin, S. Henne, E. Herrmann, N. Bukowiecki, and C. Alewell, 2015: Atmospheric ice nuclei at the high-altitude observatory Jungfraujoch, Switzerland. *Tellus*, **67B**, 25014, doi:10.3402/tellusb.v67.25014.
- Connolly, P., O. Möhler, P. Field, H. Saathoff, R. Burgess, T. Choulaton, and M. Gallagher, 2009: Studies of heterogeneous freezing by three different desert dust samples. *Atmos. Chem. Phys.*, **9**, 2805–2824, doi:10.5194/acp-9-2805-2009.
- Cozic, J., S. Mertes, B. Verheggen, D. J. Cziczo, S. J. Gallavardin, S. Walter, U. Baltensperger, and E. Weingartner, 2008: Black carbon enrichment in atmospheric ice particle residuals observed in lower tropospheric mixed phase clouds. *J. Geophys. Res.*, **113**, D15209, doi:10.1029/2007JD009266.
- Crawford, I., N. H. Robinson, M. J. Flynn, V. E. Foot, M. W. Gallagher, J. A. Huffman, W. R. Stanley, and P. H. Kaye, 2014: Characterisation of bioaerosol emissions from a Colorado pine forest: Results from the BEACHON-RoMBAS experiment. *Atmos. Chem. Phys.*, **14**, 8559–8578, doi:10.5194/acp-14-8559-2014.
- , S. Ruske, D. O. Topping, and M. W. Gallagher, 2015: Evaluation of hierarchical agglomerative cluster analysis methods for discrimination of primary biological aerosol. *Atmos. Meas. Tech.*, **8**, 4979–4991, doi:10.5194/amt-8-4979-2015.
- , and Coauthors, 2016: Observations of fluorescent aerosol-cloud interactions in the free troposphere at the High-Altitude Research Station Jungfraujoch. *Atmos. Chem. Phys.*, **16**, 2273–2284, doi:10.5194/acp-16-2273-2016.
- Cziczo, D. J., and Coauthors, 2013: Clarifying the dominant sources and mechanisms of cirrus cloud formation. *Science*, **340**, 1320–1324, doi:10.1126/science.1234145.
- , and K. D. Froyd, 2014: Sampling the composition of cirrus ice residuals. *Atmos. Res.*, **142**, 15–31, doi:10.1016/j.atmosres.2013.06.012.
- Dall’Osto, M., R. M. Harrison, E. J. Highwood, C. O’Dowd, D. Ceburnis, X. Querol, and E. P. Achterberg, 2010: Variation of the mixing state of Saharan dust particles with atmospheric transport. *Atmos. Environ.*, **44**, 3135–3146, doi:10.1016/j.atmosenv.2010.05.030.

- DeMott, P. J., D. J. Cziczo, A. J. Prenni, D. M. Murphy, S. M. Kreidenweis, D. S. Thomson, R. Borys, and D. C. Rogers, 2003a: Measurements of the concentration and composition of nuclei for cirrus formation. *Proc. Natl. Acad. Sci. USA*, **100**, 14 655–14 660, doi:10.1073/pnas.2532677100.
- , K. Sassen, M. Poellot, D. Baumgardner, D. Rogers, S. Brooks, A. Prenni, and S. Kreidenweis, 2003b: African dust aerosols as atmospheric ice nuclei. *Geophys. Res. Lett.*, **30**, 1732, doi:10.1029/2003GL017410.
- , and Coauthors, 2010: Predicting global atmospheric ice nuclei distributions and their impacts on climate. *Proc. Natl. Acad. Sci. USA*, **107**, 11 217–11 222, doi:10.1073/pnas.0910818107.
- Després, V., and Coauthors, 2012: Primary biological aerosol particles in the atmosphere: A review. *Tellus*, **64B**, 15598, doi:10.3402/tellusb.v64i0.15598.
- Diehl, K., C. Quick, S. Matthias-Maser, S. Mitra, and R. Jaenicke, 2001: The ice nucleating ability of pollen: Part I: Laboratory studies in deposition and condensation freezing modes. *Atmos. Res.*, **58**, 75–87, doi:10.1016/S0169-8095(01)00091-6.
- Ellison, G. B., A. F. Tuck, and V. Vaida, 1999: Atmospheric processing of organic aerosols. *J. Geophys. Res.*, **104**, 11 633–11 641, doi:10.1029/1999JD900073.
- Fan, J., and Coauthors, 2014: Aerosol impacts on California winter clouds and precipitation during CalWater 2011: Local pollution versus long-range transported dust. *Atmos. Chem. Phys.*, **14**, 81–101, doi:10.5194/acp-14-81-2014.
- Faure, G., 1986: *Principles of Isotope Geology*. 2nd ed. John Wiley & Sons, Inc., 608 pp.
- Gerber, H., 1991: Direct measurement of suspended particulate volume concentration and far-infrared extinction coefficient with a laser-diffraction instrument. *Appl. Opt.*, **30**, 4824–4831, doi:10.1364/AO.30.004824.
- Hande, L. B., C. Engler, C. Hoose, and I. Tegen, 2015: Seasonal variability of Saharan desert dust and ice nucleating particles over Europe. *Atmos. Chem. Phys.*, **15**, 4389–4397, doi:10.5194/acp-15-4389-2015.
- Healy, D. A., D. J. O'Connor, and J. R. Sodeau, 2012: Measurement of the particle counting efficiency of the “Waveband Integrated Bioaerosol Sensor” model number 4 (WIBS-4). *J. Aerosol Sci.*, **47**, 94–99, doi:10.1016/j.jaerosci.2012.01.003.
- Herrmann, E., and Coauthors, 2015: Analysis of long-term aerosol size distribution data from Jungfraujoch with emphasis on free tropospheric conditions, cloud influence, and air mass transport. *J. Geophys. Res. Atmos.*, **120**, 9459–9480, doi:10.1002/2015JD023660.
- Hiranuma, N., and Coauthors, 2015: A comprehensive laboratory study on the immersion freezing behavior of illite NX particles: A comparison of 17 ice nucleation measurement techniques. *Atmos. Chem. Phys.*, **15**, 2489–2518, doi:10.5194/acp-15-2489-2015.
- Hodell, D. A., G. A. Mead, and P. A. Mueller, 1990: Variation in the strontium isotopic composition of seawater (8 Ma to present): Implications for chemical weathering rates and dissolved fluxes to the oceans. *Chem. Geol. Isot. Geosci. Sect.*, **80**, 291–307, doi:10.1016/0168-9622(90)90011-Z.
- Hoose, C., and O. Möhler, 2012: Heterogeneous ice nucleation on atmospheric aerosols: A review of results from laboratory experiments. *Atmos. Chem. Phys.*, **12**, 9817–9854, doi:10.5194/acp-12-9817-2012.
- , J. E. Kristjánsson, and S. M. Burrows, 2010: How important is biological ice nucleation in clouds on a global scale? *Environ. Res. Lett.*, **5**, 024009, doi:10.1088/1748-9326/5/2/024009.
- Jaeglé, L., D. J. Jacob, Y. Wang, A. J. Weinheimer, B. Ridley, T. L. Campos, G. W. Sachse, and D. E. Hagen, 1998: Sources and chemistry of NO<sub>x</sub> in the upper troposphere over the United States. *Geophys. Res. Lett.*, **25**, 1705–1708, doi:10.1029/97GL03591.
- Kamphus, M., and Coauthors, 2010: Chemical composition of ambient aerosol, ice residues and cloud droplet residues in mixed-phase clouds: Single particle analysis during the Cloud and Aerosol Characterization Experiment (CLACE 6). *Atmos. Chem. Phys.*, **10**, 8077–8095, doi:10.5194/acp-10-8077-2010.
- Kanji, Z. A., and J. P. D. Abbatt, 2006: Laboratory studies of ice formation via deposition mode nucleation onto mineral dust and n-hexane soot samples. *J. Geophys. Res.*, **111**, D16204, doi:10.1029/2005JD006766.
- , A. Welti, C. Chou, O. Stetzer, and U. Lohmann, 2013: Laboratory studies of immersion and deposition mode ice nucleation of ozone aged mineral dust particles. *Atmos. Chem. Phys.*, **13**, 9097–9118, doi:10.5194/acp-13-9097-2013.
- Kaye, P., W. R. Stanley, E. Hirst, E. V. Foot, K. L. Baxter, and S. J. Barrington, 2005: Single particle multichannel bioaerosol fluorescence sensor. *Opt. Express*, **13**, 3583–3593, doi:10.1364/OPEX.13.003583.
- Ketterer, C., P. Zieger, N. Bukowiecki, M. Collaud Coen, O. Maier, D. Ruffieux, and E. Weingartner, 2014: Investigation of the planetary boundary layer in the Swiss Alps using remote sensing and in situ measurements. *Bound.-Layer Meteor.*, **151**, 317–334, doi:10.1007/s10546-013-9897-8.
- Klein, H., and Coauthors, 2010: Saharan dust and ice nuclei over Central Europe. *Atmos. Chem. Phys.*, **10**, 10 211–10 221, doi:10.5194/acp-10-10211-2010.
- Knopf, D. A., and T. Koop, 2006: Heterogeneous nucleation of ice on surrogates of mineral dust. *J. Geophys. Res.*, **111**, D12201, doi:10.1029/2005JD006894.
- , P. A. Alpert, B. Wang, R. E. O'Brien, S. T. Kelly, A. Laskin, M. K. Gilles, and R. C. Moffet, 2014: Microspectroscopic imaging and characterization of individually identified ice nucleating particles from a case field study. *J. Geophys. Res. Atmos.*, **119**, 10 365–10 381, doi:10.1002/2014JD021866.
- Kulkarni, P., P. Baron, and K. Willeke, Eds., 2011: *Aerosol Measurement: Principles, Techniques, and Applications*. 3rd ed. John Wiley & Sons, Inc., 883 pp., doi:10.1002/9781118001684.
- Kupiszewski, P., and Coauthors, 2015: The Ice Selective Inlet: A novel technique for exclusive extraction of pristine ice crystals in mixed-phase clouds. *Atmos. Meas. Tech.*, **8**, 3087–3106, doi:10.5194/amt-8-3087-2015.
- Lamb, D., and J. Verlinde, 2011: *Physics and Chemistry of Clouds*. Cambridge University Press, 600 pp.
- Lance, S., C. A. Brock, D. Rogers, and J. Gordon, 2010: Water droplet calibration of the Cloud Droplet Probe (CDP) and in-flight performance in liquid, ice and mixed-phase clouds during ARCPAC. *Atmos. Meas. Tech.*, **3**, 1683–1706, doi:10.5194/amt-3-1683-2010.
- Levin, Z., and S. A. Yankofsky, 1983: Contact versus immersion freezing of freely suspended droplets by bacterial ice nuclei. *J. Climate Appl. Meteor.*, **22**, 1964–1966, doi:10.1175/1520-0450(1983)022<1964:CVIFOF>2.0.CO;2.
- Li, J.-L. F., and Coauthors, 2012: An observationally based evaluation of cloud ice water in CMIP3 and CMIP5 GCMs and contemporary reanalyses using contemporary satellite data. *J. Geophys. Res.*, **117**, D16105, doi:10.1029/2012JD017640.
- Lloyd, G., and Coauthors, 2015: The origins of ice crystals measured in mixed-phase clouds at the high-alpine site Jungfraujoch.

- Atmos. Chem. Phys.*, **15**, 12 953–12 969, doi:[10.5194/acp-15-12953-2015](https://doi.org/10.5194/acp-15-12953-2015).
- Lohmann, U., and B. Kärcher, 2002: First interactive simulations of cirrus clouds formed by homogeneous freezing in the ECHAM general circulation model. *J. Geophys. Res.*, **107**, AAC 8-1–AAC 8-13, doi:[10.1029/2001JD000767](https://doi.org/10.1029/2001JD000767).
- López, M. L., and E. E. Ávila, 2013: Measurements of natural deposition ice nuclei in Córdoba, Argentina. *Atmos. Chem. Phys.*, **13**, 3111–3119, doi:[10.5194/acp-13-3111-2013](https://doi.org/10.5194/acp-13-3111-2013).
- Lugauer, M., U. Baltensperger, M. Furger, H. W. Gäggeler, D. T. Jost, M. Schwikowski, and H. Wanner, 1998: Aerosol transport to the high Alpine sites Jungfraujoch (3454 m asl) and Colle Gnifetti (4452 m asl). *Tellus*, **50B**, 76–92, doi:[10.1034/j.1600-0889.1998.00006.x](https://doi.org/10.1034/j.1600-0889.1998.00006.x).
- Maki, L., and K. J. Willoughby, 1978: Bacteria as biogenic sources of freezing nuclei. *J. Appl. Meteor.*, **17**, 1049–1053, doi:[10.1175/1520-0450\(1978\)017<1049:BABSOF>2.0.CO;2](https://doi.org/10.1175/1520-0450(1978)017<1049:BABSOF>2.0.CO;2).
- Manly, B. F., 2001: *Statistics for Environmental Science and Management*. Chapman and Hall/CRC, 336 pp.
- Marcolli, C., 2014: Deposition nucleation viewed as homogeneous or immersion freezing in pores and cavities. *Atmos. Chem. Phys.*, **14**, 2071–2104, doi:[10.5194/acp-14-2071-2014](https://doi.org/10.5194/acp-14-2071-2014).
- Mason, R. H., and Coauthors, 2015: The micro-orifice uniform deposit impactor–droplet freezing technique (MOUDI–DFT) for measuring concentrations of ice nucleating particles as a function of size: Improvements and initial validation. *Atmos. Meas. Tech.*, **8**, 2449–2462, doi:[10.5194/amt-8-2449-2015](https://doi.org/10.5194/amt-8-2449-2015).
- , and Coauthors, 2016: Size-resolved measurements of ice-nucleating particles at six locations in North America and one in Europe. *Atmos. Chem. Phys.*, **16**, 1637–1651, doi:[10.5194/acp-16-1637-2016](https://doi.org/10.5194/acp-16-1637-2016).
- McCluskey, C. S., and Coauthors, 2014: Characteristics of atmospheric ice nucleating particles associated with biomass burning in the US: Prescribed burns and wildfires. *J. Geophys. Res.*, **119**, 10 458–10 470, doi:[10.1002/2014JD021980](https://doi.org/10.1002/2014JD021980).
- Möhler, O., and Coauthors, 2008: Heterogeneous ice nucleation activity of bacteria: New laboratory experiments at simulated cloud conditions. *Biogeosciences*, **5**, 1425–1435, doi:[10.5194/bg-5-1425-2008](https://doi.org/10.5194/bg-5-1425-2008).
- Novosselov, I., and P. C. Ariessohn, 2014: Rectangular slit atmospheric pressure aerodynamic lens aerosol concentrator. *Aerosol Sci. Technol.*, **48**, 163–172, doi:[10.1080/02786826.2013.865832](https://doi.org/10.1080/02786826.2013.865832).
- Pandey Deolal, S., D. Brunner, M. Steinbacher, U. Weers, and J. Staehelin, 2012: Long-term in situ measurements of NO<sub>x</sub> and NO<sub>y</sub> at Jungfraujoch 1998–2009: Time series analysis and evaluation. *Atmos. Chem. Phys.*, **12**, 2551–2566, doi:[10.5194/acp-12-2551-2012](https://doi.org/10.5194/acp-12-2551-2012).
- , J. Staehelin, D. Brunner, J. Cui, M. Steinbacher, C. Zellweger, S. Henne, and M. K. Vollmer, 2013: Transport of PAN and NO<sub>y</sub> from different source regions to the Swiss high alpine site Jungfraujoch. *Atmos. Environ.*, **64**, 103–115, doi:[10.1016/j.atmosenv.2012.08.021](https://doi.org/10.1016/j.atmosenv.2012.08.021).
- , S. Henne, L. Ries, S. Gilge, U. Weers, M. Steinbacher, J. Staehelin, and T. Peter, 2014: Analysis of elevated spring-time levels of Peroxyacetyl nitrate (PAN) at the high Alpine research sites Jungfraujoch and Zugspitze. *Atmos. Chem. Phys.*, **14**, 12 553–12 571, doi:[10.5194/acp-14-12553-2014](https://doi.org/10.5194/acp-14-12553-2014).
- Parlanti, E., K. Wörz, L. Geoffroy, and M. Lamotte, 2000: Dissolved organic matter fluorescence spectroscopy as a tool to estimate biological activity in a coastal zone submitted to anthropogenic inputs. *Org. Geochem.*, **31**, 1765–1781, doi:[10.1016/S0146-6380\(00\)00124-8](https://doi.org/10.1016/S0146-6380(00)00124-8).
- Petters, M. D., and Coauthors, 2009: Ice nuclei emissions from biomass burning. *J. Geophys. Res.*, **114**, D07209, doi:[10.1029/2008JD011532](https://doi.org/10.1029/2008JD011532).
- Phillips, V. T. J., P. J. Demott, C. Andronache, K. A. Pratt, K. A. Prather, R. Subramanian, and C. Twohy, 2013: Improvements to an empirical parameterization of heterogeneous ice nucleation and its comparison with observations. *J. Atmos. Sci.*, **70**, 378–409, doi:[10.1175/JAS-D-12-080.1](https://doi.org/10.1175/JAS-D-12-080.1).
- Pöhlker, C., J. A. Huffman, and U. Pöschl, 2012: Autofluorescence of atmospheric bioaerosols—Fluorescent biomolecules and potential interferences. *Atmos. Meas. Tech.*, **5**, 37–71, doi:[10.5194/amt-5-37-2012](https://doi.org/10.5194/amt-5-37-2012).
- Pöschl, U., Y. Rudich, and M. Ammann, 2007: Kinetic model framework for aerosol and cloud surface chemistry and gas-particle interactions—Part 1: General equations, parameters, and terminology. *Atmos. Chem. Phys.*, **7**, 5989–6023, doi:[10.5194/acp-7-5989-2007](https://doi.org/10.5194/acp-7-5989-2007).
- Prenni, A. J., P. J. DeMott, D. C. Rogers, S. Kreidenweis, G. M. McFarquhar, and G. Zhang, 2009: Ice nuclei characteristics from M-PACE and their relation to ice formation in clouds. *Tellus*, **61B**, 436–448, doi:[10.1111/j.1600-0889.2009.00415.x](https://doi.org/10.1111/j.1600-0889.2009.00415.x).
- Pruppacher, H. R., and J. D. Klett, 1997: *Microphysics of Clouds and Precipitation*. Atmospheric and Oceanographic Sciences Library, Vol. 18, Kluwer Academic Publishers, 954 pp., doi:[10.1007/978-0-306-48100-0](https://doi.org/10.1007/978-0-306-48100-0).
- Rogers, D., P. J. DeMott, S. M. Kreidenweis, and Y. Chen, 1998: Measurements of ice nucleating aerosols during SUCCESS. *Geophys. Res. Lett.*, **25**, 1383–1386, doi:[10.1029/97GL03478](https://doi.org/10.1029/97GL03478).
- , —, —, and —, 2001: A continuous-flow diffusion chamber for airborne measurements of ice nuclei. *J. Atmos. Oceanic Technol.*, **18**, 725–741, doi:[10.1175/1520-0426\(2001\)018<0725:ACFDCF>2.0.CO;2](https://doi.org/10.1175/1520-0426(2001)018<0725:ACFDCF>2.0.CO;2).
- Rogers, R., and M. Yau, 1989: *A Short Course in Cloud Physics*. 3rd ed. Pergamon, 304 pp.
- Salam, A., U. Lohmann, and G. Lesins, 2007: Ice nucleation of ammonia gas exposed montmorillonite mineral dust particles. *Atmos. Chem. Phys.*, **7**, 3923–3931, doi:[10.5194/acp-7-3923-2007](https://doi.org/10.5194/acp-7-3923-2007).
- Santachiara, G., L. Di Matteo, F. Prodi, and F. Belosi, 2010: Atmospheric particles acting as ice forming nuclei in different size ranges. *Atmos. Res.*, **96**, 266–272, doi:[10.1016/j.atmosres.2009.08.004](https://doi.org/10.1016/j.atmosres.2009.08.004).
- Seinfeld, J. H., and S. P. Pandis, 2006: *Atmospheric Chemistry and Physics: From Air Pollution to Climate Change*. 2nd ed. John Wiley & Sons, Inc., 1232 pp.
- Stedmon, C. A., S. Markager, and R. Bro, 2003: Tracing dissolved organic matter in aquatic environments using a new approach to fluorescence spectroscopy. *Mar. Chem.*, **82**, 239–254, doi:[10.1016/S0304-4203\(03\)00072-0](https://doi.org/10.1016/S0304-4203(03)00072-0).
- Stein, M., A. Starinsky, A. Katz, S. Goldstein, M. Machlus, and A. Schramm, 1997: Strontium isotopic, chemical, and sedimentological evidence for the evolution of Lake Lisan and the Dead Sea. *Geochim. Cosmochim. Acta*, **61**, 3975–3992, doi:[10.1016/S0016-7037\(97\)00191-9](https://doi.org/10.1016/S0016-7037(97)00191-9).
- Steinbacher, M., L. Emmenegger, and C. Hueglin, 2015: National Air Pollution Monitoring Network (NABEL). International Foundation High Altitude Research Stations Jungfraujoch and Gornergrat Activity Rep. 2014, 85–88. [Available online at [http://www.ifjngo.ch/reports/2014/pdf/124\\_Empa\\_Hueglin\\_cf.pdf](http://www.ifjngo.ch/reports/2014/pdf/124_Empa_Hueglin_cf.pdf)].
- Stohl, A., C. Forster, A. Frank, P. Seibert, and G. Wotawa, 2005: Technical note: The Lagrangian particle dispersion model FLEXPART version 6.2. *Atmos. Chem. Phys.*, **5**, 2461–2474, doi:[10.5194/acp-5-2461-2005](https://doi.org/10.5194/acp-5-2461-2005).

- Stopelli, E., F. Conen, C. E. Morris, E. Herrmann, N. Bukowiecki, and C. Alewell, 2015: Ice nucleation active particles are efficiently removed by precipitating clouds. *Sci. Rep.*, **5**, 16433, doi:10.1038/srep16433.
- Sturm, P., B. Tuzson, S. Henne, and L. Emmenegger, 2013: Tracking isotopic signatures of CO<sub>2</sub> at the high altitude site Jungfraujoch with laser spectroscopy: Analytical improvements and representative results. *Atmos. Meas. Tech.*, **6**, 1659–1671, doi:10.5194/amt-6-1659-2013.
- Sullivan, R. C., and Coauthors, 2010: Irreversible loss of ice nucleation active sites in mineral dust particles caused by sulphuric acid condensation. *Atmos. Chem. Phys.*, **10**, 11 471–11 487, doi:10.5194/acp-10-11471-2010.
- Targino, A., and Coauthors, 2009: Influence of particle chemical composition on the phase of cold clouds at a high-alpine site in Switzerland. *J. Geophys. Res.*, **114**, D18206, doi:10.1029/2008JD011365.
- Vochezer, P., E. Järvinen, R. Wagner, P. Kupiszewski, T. Leisner, and M. Schnaiter, 2016: In situ characterization of mixed phase clouds using the Small Ice Detector and the Particle Phase Discriminator. *Atmos. Meas. Tech.*, **9**, 159–177, doi:10.5194/amt-9-159-2016.
- Voerkelius, S., and Coauthors, 2010: Strontium isotopic signatures of natural mineral waters, the reference to a simple geological map and its potential for authentication of food. *Food Chem.*, **118**, 933–940, doi:10.1016/j.foodchem.2009.04.125.
- Wagner, R., O. Möhler, H. Saathoff, and M. Schnaiter, 2014: Enhanced high-temperature ice nucleation ability of crystallized aerosol particles after preactivation at low temperature. *J. Geophys. Res. Atmos.*, **119**, 8212–8230, doi:10.1002/2014JD021741.
- Weingartner, E., S. Nyeki, and U. Baltensperger, 1999: Seasonal and diurnal variation of aerosol size distributions (10 < D < 750 nm) at a high-alpine site (Jungfraujoch 3580 m asl). *J. Geophys. Res.*, **104**, 26 809–26 820, doi:10.1029/1999JD900170.
- Wendisch, M., T. J. Garrett, and J. W. Strapp, 2002: Wind tunnel tests of the airborne PVM-100A response to large droplets. *J. Atmos. Oceanic Technol.*, **19**, 1577–1584, doi:10.1175/1520-0426(2002)019<1577:WTTOTA>2.0.CO;2.
- Wernli, B., and H. Davies, 1997: A Lagrangian-based analysis of extratropical cyclones. I: The method and some applications. *Quart. J. Roy. Meteor. Soc.*, **123**, 467–489, doi:10.1002/qj.49712353811.
- Wex, H., and Coauthors, 2014: Kaolinite particles as ice nuclei: Learning from the use of different kaolinite samples and different coatings. *Atmos. Chem. Phys.*, **14**, 5529–5546, doi:10.5194/acp-14-5529-2014.
- , and Coauthors, 2015: Intercomparing different devices for the investigation of ice nucleating particles using Snomax as test substance. *Atmos. Chem. Phys.*, **15**, 1463–1485, doi:10.5194/acp-15-1463-2015.
- Wilson, T. W., and Coauthors, 2015: A marine biogenic source of atmospheric ice-nucleating particles. *Nature*, **525**, 234–238, doi:10.1038/nature14986.
- Worringen, A., and Coauthors, 2015: Single-particle characterization of ice-nucleating particles and ice particle residuals sampled by three different techniques. *Atmos. Chem. Phys.*, **15**, 4161–4178, doi:10.5194/acp-15-4161-2015.
- Yakobi-Hancock, J. D., L. A. Ladino, and J. P. D. Abbatt, 2013: Feldspar minerals as efficient deposition ice nuclei. *Atmos. Chem. Phys.*, **13**, 11 175–11 185, doi:10.5194/acp-13-11175-2013.
- Yang, Z., A. K. Bertram, and K. C. Chou, 2011: Why do sulfuric acid coatings influence the ice nucleation properties of mineral dust particles in the atmosphere? *J. Phys. Chem. Lett.*, **2**, 1232–1236, doi:10.1021/jz2003342.
- Zellweger, C., J. Forrer, P. Hofer, S. Nyeki, B. Schwarzenbach, E. Weingartner, M. Ammann, and U. Baltensperger, 2003: Partitioning of reactive nitrogen (NO<sub>x</sub>) and dependence on meteorological conditions in the lower free troposphere. *Atmos. Chem. Phys.*, **3**, 779–796, doi:10.5194/acp-3-779-2003.
- , M. Steinbacher, and B. Buchmann, 2012: Evaluation of new laser spectrometer techniques for in-situ carbon monoxide measurements. *Atmos. Meas. Tech.*, **5**, 2555–2567, doi:10.5194/amt-5-2555-2012.